

1 **Decadal change of summertime reactive oxidized nitrogen and surface**
2 **ozone over the Southeast United States**

3 Jingyi Li¹, Jingqiu Mao², Arlene M. Fiore³, Ronald C. Cohen^{4,5}, John D. Crouse⁶, Alex
4 P. Teng⁶, Paul O. Wennberg^{6,7}, Ben H. Lee⁸, Felipe D. Lopez-Hilfiker⁸, Joel A.
5 Thornton⁸, Jeff Peischl^{9,10}, Ilana B. Pollack¹¹, Thomas B. Ryerson⁹, Patrick Veres^{9,10},
6 James M. Roberts⁹, J. Andrew Neuman^{9,10}, John B. Nowak^{12,a}, Glenn M. Wolfe^{13,14},
7 Thomas F. Hanisco¹⁴, Alan Fried¹⁵, Hanwant B. Singh¹⁶, Jack Dibb¹⁷, Fabien Paulot^{18,19},
8 Larry W. Horowitz¹⁹

9
10 ¹Jiangsu Key Laboratory of Atmospheric Environment Monitoring and Pollution Control, Collaborative
11 Innovation Center of Atmospheric Environment and Equipment Technology, School of Environmental
12 Science and Engineering, Nanjing University of Information Science and Technology, Nanjing, Jiangsu,
13 210044, China

14 ²Department of Chemistry and Biochemistry & Geophysical Institute, University of Alaska Fairbanks,
15 Fairbanks, Alaska, 99775, USA

16 ³Department of Earth and Environmental Sciences & Lamont-Doherty Earth Observatory of Columbia
17 University, Palisades, New York, 10027, USA

18 ⁴Department of Chemistry, University of California, Berkeley, Berkeley, California, 94720, USA

19 ⁵Department of Earth and Planetary Science, University of California, Berkeley, Berkeley, California,
20 94720, USA

21 ⁶Division of Geological and Planetary Sciences, California Institute of Technology, Pasadena, California,
22 91125, USA

23 ⁷Division of Engineering and Applied Science, California Institute of Technology, Pasadena, California,
24 91125, USA

25 ⁸Department of Atmospheric Sciences, University of Washington, Seattle, Washington, 98195, USA

26 ⁹Chemical Sciences Division, NOAA Earth System Research Laboratory, Boulder, Colorado, 80305, USA

27 ¹⁰Cooperative Institute for Research in Environmental Science, University of Colorado Boulder, Boulder,
28 Colorado, 80309, USA

29 ¹¹Department of Atmospheric Science, Colorado State University, Fort Collins, Colorado, 80523, USA

30 ¹²Aerodyne Research, Inc., Billerica, Massachusetts, 01821, USA

31 ¹³Joint Center for Earth System Technology, University of Maryland Baltimore County, Baltimore,
32 Maryland, 21250, USA

33 ¹⁴Atmospheric Chemistry and Dynamics Lab, NASA Goddard Space Flight Center, Greenbelt, Maryland,
34 20771, USA

35 ¹⁵Institute of Arctic & Alpine Research, University of Colorado, Boulder, Colorado, 80309, USA

36 ¹⁶NASA Ames Research Center, Moffett Field, California, 94035, USA

37 ¹⁷Department of Earth Sciences and Institute for the Study of Earth, Oceans, and Space, University of New
38 Hampshire, Durham, New Hampshire, 03824, USA

39 ¹⁸Program in Atmospheric and Oceanic Sciences, Princeton University, Princeton, New Jersey, 08544,
40 USA

41 ¹⁹Geophysical Fluid Dynamics Laboratory/National Oceanic and Atmospheric Administration, Princeton,
42 New Jersey, 08540, USA

43 ^anow at: NASA Langley Research Center, Hampton, Virginia, USA

44
45 Correspondence to: Jingqiu Mao (jmao2@alaska.edu)

46

47 **Abstract**

48 Widespread efforts to abate ozone (O_3) smog have significantly reduced nitrogen oxides
49 (NO_x) emissions over the past two decades in the Southeast U.S. (SEUS), a place heavily
50 influenced by both anthropogenic and biogenic emissions. How reactive nitrogen
51 speciation responds to the reduction in NO_x emissions in this region remains to be
52 elucidated. Here we exploit aircraft measurements from ICARTT (July-August, 2004),
53 SENEX (June-July, 2013), and SEAC⁴RS (August-September, 2013) and long-term
54 ground measurement networks alongside a global chemistry-climate model to examine
55 decadal changes in summertime reactive oxidized nitrogen (RON) and ozone over the
56 Southeast U.S. We show that our model can well reproduce the mean vertical profiles of major
57 RON species and the total (NO_y) in both 2004 and 2013. Among the major RON species, nitric
58 acid (HNO_3) is dominated ($\sim 42 - 45\%$), followed by NO_x (31%), total peroxy nitrates (ΣPNs ;
59 14%), and total alkyl nitrates (ΣANs ; 9 – 12%) on a regional scale. We find that most RON,
60 including NO_x , ΣPNs and HNO_3 decline proportionally with decreasing NO_x emissions in
61 this region, leading to a similar decline in NO_y . This linear response might be in part due
62 to the nearly constant summertime supply of biogenic VOC emissions in this region. Our
63 model captures the observed relative change of RON and surface ozone from 2004 to 2013.
64 Model sensitivity tests indicate that further reductions of NO_x emissions will lead to a
65 continued decline in surface ozone and less frequent high ozone events.

66 **1 Introduction**

67 Since the 1990s, the U.S.A. Environmental Protection Agency (U.S. EPA) has targeted
68 emissions of nitrogen oxides (NO_x) to improve air quality by lowering regional
69 photochemical smog (The 1990 Clean Air Amendment). Satellite- and ground-based
70 observations imply significant declines in U.S. NO_x emissions, with a decreasing rate of
71 roughly $-4\% \text{ yr}^{-1}$ after 2005 (Krotkov et al., 2016; Russell et al., 2012; Tong et al., 2015;
72 Miyazaki et al., 2017; Lu et al., 2015; Lamsal et al., 2015). This has proven effective at
73 lowering near-surface ozone (O_3) in the past few decades (Cooper et al., 2012; Simon et
74 al., 2015; Hidy and Blanchard, 2015; Stoeckenius et al., 2015; Xing et al., 2015; Yahya et
75 al., 2016; Astitha et al., 2017). The average of the annual 4th highest daily maximum 8-h
76 average (MDA8) ozone over 206 sites has decreased by 31% from 101 ppb in 1980 to 70
77 ppb in 2016 across the continental U.S., with more significant reductions in rural areas of
78 the eastern U.S. in summer (Simon et al., 2015; Cooper et al., 2012). Here we use both
79 aircraft and ground-based datasets, combined with a high resolution chemistry-climate
80 model, to evaluate responses of reactive oxidized nitrogen (RON) and surface ozone to the
81 NO_x emission reductions in the Southeast U.S.

82 In the troposphere, ozone is produced through photochemical reactions involving NO_x and
83 volatile organic compounds (VOCs) in the presence of sunlight. During photooxidation, a
84 large fraction of NO_x is transformed into its reservoirs, including nitric acid (HNO_3),

85 peroxy nitrates (RO_2NO_2 ; dominated by peroxyacetyl nitrate (PAN)), and alkyl nitrates
86 (RONO_2). These species, together with NO_x , are known as total reactive oxidized nitrogen
87 ($\text{NO}_y = \text{NO}_x + \text{HNO}_3 + \text{HONO} + 2 \times \text{N}_2\text{O}_5 + \text{total peroxy nitrates} (\Sigma\text{PNs}) + \text{total alkyl}$
88 $\text{nitrates} (\Sigma\text{ANs})$). Some of these reservoir species, particularly those with an organic
89 component, tend to be less soluble and longer lived. They may carry reactive nitrogen far
90 from the NO_x source region (Stohl et al., 2002; Parrish et al., 2004; Li et al., 2004) and
91 thereby affect NO_x concentrations and O_3 formation on a regional to global scale (Liang et
92 al., 1998; Horowitz et al., 1998; Perring et al., 2013; Paulot et al., 2016; Hudman et al.,
93 2004).

94 RONO_2 originating from biogenic VOCs (BVOCs) represents a major uncertainty in the
95 NO_y budget, as BVOC emissions account for more than 80 % of global VOC emissions
96 (Millet et al., 2008). To a large extent, this is due to the uncertainties in current
97 understanding of BVOC oxidation chemistry. Biogenic RONO_2 species are mainly
98 produced from the oxidation of BVOCs by OH in the presence of NO_x during daytime and
99 by nitrate radical (NO_3) during nighttime. Laboratory and field studies show a wide range
100 of RONO_2 yields from their BVOC precursors (Browne et al., 2014; Fry et al., 2014;
101 Lockwood et al., 2010; Paulot et al., 2009; Rindelaub et al., 2015; Rollins et al., 2009; Lee
102 et al., 2014; Xiong et al., 2015; Xiong et al., 2016; Teng et al., 2015). Another uncertainty
103 lies in the fate of RONO_2 , i.e. recycling RONO_2 into NO_x or converting it to HNO_3 have
104 important implications for the NO_y budget and thus O_3 production (Fiore et al., 2005;
105 Horowitz et al., 2007; Ito et al., 2009; Perring et al., 2013; Paulot et al., 2012). This is
106 further complicated by particle-phase RONO_2 , an important component of secondary
107 organic aerosol (SOA) over the Southeast U.S. (Xu et al., 2015; Lee et al., 2016). The fate
108 of particle-phase RONO_2 is unclear, with the possibility for removal by hydrolysis to form
109 HNO_3 (Jacobs et al., 2014; Hu et al., 2011; Darer et al., 2011; Rindelaub et al., 2015;
110 Szmigielski et al., 2010; Sato, 2008; Romer et al., 2016; Wolfe et al., 2015), photochemical
111 aging (Nah et al., 2016; Boyd et al., 2015), and deposition (Nguyen et al., 2015). To what
112 extent RONO_2 affect the partitioning of RON and surface ozone remains to be elucidated.

113 Extensive datasets in the Southeast U.S. offer a great opportunity to study the decadal
114 change of RON and surface ozone, resulting from NO_x emission decline. Aircraft
115 campaigns during the summers of 2004 and 2013, including the International Consortium
116 for Atmospheric Research on Transport and Transformation (ICARTT) (Fehsenfeld et al.,
117 2006; Singh et al., 2006), the Southeast Nexus (SENEX) (Warneke et al., 2016), and the
118 Studies of Emissions and Atmospheric Composition, Clouds and Climate Coupling by
119 Regional Surveys (SEAC⁴RS) (Toon et al., 2016), provide detailed characterization of
120 tropospheric composition in this region separated by nearly a decade. These data have been
121 widely used to evaluate model estimates of RON and ozone (Singh et al., 2007; Pierce et
122 al., 2007; Perring et al., 2009; Fischer et al., 2014; Hudman et al., 2007; Henderson et al.,
123 2011; Hudman et al., 2009; Edwards et al., 2017; Baker and Woody, 2017; Travis et al.,

124 2016; Mao et al., 2013b; Fisher et al., 2016; Yu et al., 2016; Liu et al., 2016). Together
125 with measurements from networks, including the National Atmospheric Deposition
126 Program (NADP) and EPA Air Quality System (AQS), these datasets enable a close
127 examination of responses of RON and surface ozone to NO_x emissions reduction in this
128 region.

129 Here we use a high-resolution global 3D climate-chemistry model, the Geophysical Fluid
130 Dynamics Laboratory (GFDL) AM3 model, with updated isoprene and organic nitrate
131 chemistry to investigate decadal changes of RON and surface O₃ during summer between
132 2004 and 2013 over the Southeast U.S. We first evaluate the model with comprehensive
133 measurements from three aircraft campaigns in the summer of 2004 (ICARTT) and 2013
134 (SENEX and SEAC⁴RS). Model estimates of nitrate wet deposition flux are also evaluated
135 against measurements from NADP; model estimates of NO_y are compared with
136 measurements from EPA AQS to provide an additional constraint on the fate of RON in
137 the model. We then investigate the repartitioning of RON in response to NO_x emission
138 reductions from 2004 to 2013 on a regional scale. From there, we examine the model
139 estimate of decadal changes of summertime surface O₃ at 157 EPA AQS monitoring sites
140 over the Southeast U.S. We also demonstrate the sensitivity of RON and MDA8 O₃ to a
141 hypothetical NO_x emission reduction over the next decade.

142 **2 Methodology**

143 **2.1 AM3 Model**

144 We apply a high-resolution (50 x 50 km²) version of the GFDL AM3 global chemistry-
145 climate model to study decadal changes of RON and O₃ over the Southeast U.S. Chemistry-
146 climate models provide a unique capability to both evaluate model representation of these
147 observed changes and use that to improve future projections of air quality in the same
148 region. The model configuration is to a large extent similar to that used in another paper
149 (Li et al., 2016); and a short summary is provided below. The dynamical core, physical
150 parameterizations, cloud and precipitation processes, and cloud-aerosol interactions mainly
151 follow Donner et al. (2011), except that convective plumes are computed on a vertical grid
152 with finer resolution (Paulot et al., 2016). Dry deposition in the model has been updated to
153 use dry deposition velocities calculated in the GEOS-Chem model (Paulot et al., 2016), to
154 reflect rapid deposition of organic nitrates and oxidized volatile organic compounds
155 (OVOCs) (Nguyen et al., 2015). The current time step for chemistry and transport in our
156 model is 20 mins. We show below in section 4.1 that, with the current setting, our model
157 can well reproduce the vertical profiles of RON. Sensitivity of RON to operator duration
158 should refer to Philip et al. (2016).

159 Isoprene emissions are computed in the model using the Model of Emissions of Gases and
160 Aerosols from Nature (MEGAN). In 2004, isoprene emissions over the continental U.S.

161 (25-50° N, 130-70° W) are computed to be 8.0 Tg C in July and August together, with a
162 previous model estimate of 7.5 Tg C by Mao et al. (2013b). In 2013, model estimates of
163 isoprene emissions were scaled down by 20% following Li et al. (2016). The resulting
164 isoprene emissions are 7.7 Tg C in July-August in this region, with little difference
165 compared to 2004. Monoterpene emissions follow Naik et al. (2013) and do not vary
166 interannually, with a total of 4.0 Tg C in July and August.

167 Anthropogenic emissions follow the Representative Concentration Pathway 8.5 (RCP 8.5)
168 projection (Lamarque et al., 2011) for both 2004 and 2013, to compare the model to
169 observations in a consistent fashion and also enable future projection of air quality in this
170 region. As shown in Table 1, anthropogenic NO_x emissions over the continental U.S.
171 during July-August of 2004 amount to 0.42 Tg N mon⁻¹, consistent with Hudman et al.
172 (2007) but 11 % lower than EPA estimates of 0.47 Tg N mon⁻¹ (Granier et al., 2011). For
173 the year of 2013, we apply a 25 % reduction to the anthropogenic NO_x emissions from the
174 RCP 8.5 projection (from base year of 2010), to best reproduce the vertical profiles of RON
175 during SENEX as shown below in section 4.1. This adjustment is also consistent with
176 recent estimates of NO_x emissions over the Southeast U.S. (Anderson et al., 2014). The
177 resulting anthropogenic NO_x emissions (0.25 Tg N mon⁻¹) are 14 % lower than NEI11v1
178 emission inventory estimate of 0.29 Tg N mon⁻¹ (0.28 Tg N mon⁻¹ from the updated
179 NEI11v2 emission inventory), although both inventories have a similar spatial distribution
180 (Figure S1). We also apply a diurnal variation to anthropogenic NO_x emissions following
181 Mao et al. (2013b). Soil NO_x emissions in our model, 3.6 Tg N yr⁻¹ globally (Naik et al.,
182 2013), are considerably lower than other model estimates, including 5.5 Tg N yr⁻¹ in
183 Yienger and Levy (1995) and 9.0 Tg N yr⁻¹ in Hudman et al. (2012). As a result, the
184 anthropogenic NO_x emissions over the continental U.S. are 0.84 Tg N for July-August of
185 2004, and 0.50 Tg N in July-August of 2013, with 40 % reduction from 2004 to 2013
186 (Table 1). This relative change in anthropogenic NO_x emissions is consistent with EPA
187 estimates ([https://www.epa.gov/air-emissions-inventories/air-pollutant-emissions-trends-](https://www.epa.gov/air-emissions-inventories/air-pollutant-emissions-trends-data)
188 [data](https://www.epa.gov/air-emissions-inventories/air-pollutant-emissions-trends-data)) and satellite observations (Krotkov et al., 2016; Lu et al., 2015). Compared to the
189 NEI11v1 inventory, RCP 8.5 used in our model shows similar relative differences in both
190 national and Southeast region.

191 **2.2 Gas-phase chemistry**

192 We apply the same isoprene mechanism as described by Li et al. (2016). A full list of the
193 reactions can be found in Table S1. This mechanism is based on Mao et al. (2013b), but
194 has been significantly revised to incorporate recent laboratory updates on isoprene
195 oxidation by OH and O₃ (Schwantes et al., 2015; Bates et al., 2016; Peeters et al., 2014; St.
196 Clair et al., 2016; Bates et al., 2014; Praske et al., 2015; Müller et al., 2014; Lee et al., 2014;
197 Crouse et al., 2011). One major feature is the suppression of δ -isoprene hydroxyl peroxy
198 radical (δ -ISOPO₂) and subsequent reaction pathways in the model, as these channels are

199 considered to be of minor importance under ambient conditions (Peeters et al., 2014; Bates
200 et al., 2014). The fraction of ISOPO₂ undergoing isomerization is calculated using bulk
201 isomerization estimates (Crouse et al., 2011). As a result, the first-generation isoprene
202 alkyl nitrate is assumed to be β-hydroxy nitrate (ISOPNB) in the model with a yield of 10 %
203 from the ISOPO₂ + NO pathway. This differs from a recent GEOS-Chem study of organic
204 nitrates over the Southeast U.S. that assumed 9 % yield of the first-generation isoprene
205 alkyl nitrate comprised of 90 % ISOPNB and 10 % δ-hydroxy nitrate (ISOPND) (Fisher et
206 al., 2016). The treatment of β- and δ-ISOPO₂ will not only affect the speciation of organic
207 nitrates but also the production of O₃ due to different NO_x recycling efficiency in their
208 secondary products. We also include updated chemistry for methylvinyl ketone (MVK)
209 (Praske et al., 2015), an updated yield of hydroxy hydroperoxides (ISOPOOH) (Bates et
210 al., 2016; St. Clair et al., 2016), fast photolysis of carbonyl organic nitrates (Müller et al.,
211 2014), and an updated ozonolysis rate of ISOPNB (Lee et al., 2014). In addition, we reduce
212 the yield of organic nitrates (MACRN) from methacrolein (MACR) oxidation from 15 %
213 to 3 %, which is estimated from the measured yield of nitrate from MVK oxidation (Praske
214 et al., 2015).

215 Another major model revision involves the treatment of nighttime oxidation of isoprene.
216 Instead of following Mao et al. (2013b), we revised nighttime oxidation of isoprene largely
217 based on the Leeds Master Chemical Mechanism v3.2 (MCM v3.2), allowing a more
218 complete description of isoprene oxidation by NO₃. In particular, MCM v3.2 suggests
219 significant production of propanone nitrate (PROPNN) from the photooxidation of the C₅
220 carbonyl nitrate, consistent with recent laboratory experiments (Schwantes et al., 2015).
221 We also updated the products of the reaction of nitrooxy alkylperoxy radical (INO₂), the
222 peroxy radical from isoprene oxidation by NO₃, with HO₂ to reflect a lower molar yield
223 (0.77) of C₅ nitrooxy hydroperoxide (INPN) (Schwantes et al., 2015). The differences
224 between MCM v3.2 and the most updated version, MCM v3.3.1, in isoprene nighttime
225 chemistry appears to be small (Jenkin et al., 2015). We therefore use MCM v3.2 as the
226 reference in this work.

227 We include a highly simplified chemistry for the oxidation of monoterpenes in this work,
228 mainly to quantify their contribution to organic nitrates. Monoterpenes are lumped into one
229 chemical species (C₁₀H₁₆) in our model. The organic nitrate yield is set to 26 % from OH-
230 initiated oxidation (Rindelaub et al., 2015) and to 10 % from NO₃-initiated oxidation
231 (Browne et al., 2014). Details of the monoterpene chemistry can be found in Table S2.

232 **2.3 Heterogeneous loss of organic nitrates**

233 Field and laboratory studies have indicated a potential contribution to aerosol formation of
234 organic nitrates from BVOC oxidation (Ayres et al., 2015; Fry et al., 2014; Nah et al., 2016;
235 Rollins et al., 2009; Rindelaub et al., 2015; Boyd et al., 2015; Lee et al., 2016; Ng et al.,
236 2008; Fry et al., 2009; Xu et al., 2015; Lee et al., 2014; Bean and Hildebrandt Ruiz, 2016;

237 Spittler et al., 2006). Aerosol yield depends on both the VOC precursor and the oxidant.
238 For example, Δ -3-carene oxidation by NO_3 can produce a 38-65 % yield of organic aerosols
239 in a smog chamber (Fry et al., 2014), which is much higher than the 1-24 % yield from
240 NO_3 -initiated isoprene oxidation (Ng et al., 2008; Rollins et al., 2009; Ayres et al., 2015).
241 Recent chamber studies indicate a very low aerosol yield from α -pinene oxidation by NO_3
242 (Nah et al., 2016; Fry et al., 2014), the aerosol yield increases to ~ 18 % when α -pinene is
243 oxidized by OH (Rollins et al., 2010; Rindelaub et al., 2015). It should be noted that these
244 results from laboratory experiments might not be representative of atmospheric conditions
245 in terms of the RO_2 reaction partner or RO_2 lifetime.

246 In the condensed phase, organic nitrates can undergo hydrolysis reactions producing HNO_3
247 (Darer et al., 2011; Hu et al., 2011; Rindelaub et al., 2015; Boyd et al., 2015; Szmigielski
248 et al., 2010; Sato, 2008; Jacobs et al., 2014; Bean and Hildebrandt Ruiz, 2016). However,
249 the hydrolysis rate varies greatly with the structure of nitrate (Bean and Hildebrandt Ruiz,
250 2016; Darer et al., 2011; Hu et al., 2011; Boyd et al., 2015; Rindelaub et al., 2016). Here
251 we assume a first-order irreversible reactive uptake for the heterogeneous loss of organic
252 nitrates onto aerosols (R1), followed by its hydrolysis reaction returning HNO_3 and
253 alcohols (R2) (Fisher et al., 2016):



254 where RONO_2 , AONJ and ROH represent gas- and particle-phase organic nitrates and
255 alcohols respectively. We allow heterogeneous loss of organic nitrates to sulfate, black
256 carbon, primary organic carbon, sea salt, mineral dust and SOA following Mao et al.
257 (2013a). Besides the base case that only includes ISOPNB for heterogeneous loss (Jacobs
258 et al., 2014), we include two additional sensitivity tests to evaluate the potential impact of
259 organic nitrate hydrolysis. One is “hydro_full” case including heterogeneous loss of a C_5
260 dihydroxy dinitrate (DHDN) and monoterpene nitrates from OH oxidation (TERPN1), and
261 the other one is “no_hydro” case assuming no heterogeneous loss for any organic nitrates.
262 We adopt an effective uptake coefficient 0.005 for ISOPNB and DHDN, and 0.01 for
263 TERPN1, following Fisher et al. (2016), with a 3-h bulk lifetime in particle phase (Pye et
264 al., 2015; Lee et al., 2016) (Table S3). Details of each case are listed in Table 2.

265 **3 Observational datasets**

266 We use measurements from a series of field campaigns (2004 ICARTT, 2013 SENEX, and
267 2013 SEAC⁴RS) to evaluate model performance on O_3 , NO_x , HNO_3 , PAN, ΣANs and NO_y
268 over the Southeast U.S. in summer.

269 The ICARTT aircraft campaign provided a detailed characterization of tropospheric
270 chemistry over the eastern U.S. in the summer of 2004 (July 1 - August 15, 2004). Two

271 aircrafts, the NASA DC-8 and the NOAA WP-3D, were deployed to collect measurements
272 of ozone, RON, isoprene and its oxidation products. Here we focus on data including O₃,
273 NO_x, HCHO (Tunable Diode Laser (TDL) absorption spectrometry), HNO₃ (mist
274 chamber/IC by University of New Hampshire and Chemical Ionization Mass Spectrometer
275 (CIMS) by California Institute of Technology), PAN and ΣANs (including gas and aerosol
276 RONO₂) collected on the NASA DC-8 aircraft over the Southeast U.S. Details of the
277 instrument operation and accuracy are summarized in Singh et al. (2006) and references
278 therein.

279 Two aircraft campaigns were conducted in the summer of 2013 over the Southeast U.S.
280 The first one is NOAA SENEX campaign, using NOAA WP-3D aircraft to investigate the
281 interaction between biogenic and anthropogenic emissions and the formation of secondary
282 pollutants (May 27 - July 10, 2013). We focus on daytime measurements of O₃, NO_x, HNO₃,
283 PAN, speciated RONO₂ and NO_y in this work. Details of the instrument operation and
284 accuracy are summarized in Warneke et al. (2016) and references therein. The second one
285 is NASA SEAC⁴RS campaign, which took place in August - September of 2013, with a
286 focus on vertical transport of atmospheric pollutants from the surface to the stratosphere.
287 Here we focus on observations of O₃, NO₂, HCHO (laser-induced fluorescence, LIF),
288 ΣANs (including gas and aerosol RONO₂) and speciated RONO₂ collected on NASA DC-
289 8 aircraft to evaluate model representation of ΣANs and several RONO₂ originating from
290 isoprene oxidation. Details of the instrument operation and accuracy are summarized in
291 Toon et al. (2016) and references therein.

292 Besides these aircraft campaigns, we also use surface observations for model evaluation,
293 including nitrate (NO₃⁻) wet deposition flux and concentration from the National Trends
294 Network (NTN) of NADP (accessible at <http://nadp.sws.uiuc.edu/data/>) and surface O₃ and
295 NO_y from EPA AQS (accessible at
296 https://aqz.epa.gov/aqzweb/documents/data_mart_welcome.html). We focus on NO₃⁻ wet
297 deposition fluxes at 53 NADP sites (Figure 3) and MDA8 O₃ at 157 EPA AQS sites (Figure
298 S3) in the Southeast U.S. during July - August of 2004 and 2013. NO_y measurements at 10
299 out of the 157 AQS sites in the same episodes are compared with model estimates as an
300 additional constraint on the decadal change of NO_y. We choose July – August as our
301 ‘summer’ since this is the common period of all the measurements used in model
302 evaluation.

303 **4 Model evaluation**

304 We evaluate our model against observations from aircraft campaigns in 2004 and 2013.
305 For each of the three field campaigns, all measurements are averaged to a 1-min time
306 resolution. Data from biomass burning (CH₃CN ≥ 225 ppt or HCN ≥ 500 ppt), urban
307 plumes (NO₂ ≥ 4 ppb or NO_x/NO_y ≥ 0.4 (if NO_y is available)), and stratospheric air

308 ($O_3/CO > 1.25$ mol mol⁻¹) are excluded (Hudman et al., 2007) in all the analyses, as these
309 subgrid processes may not be well represented in our model. We focus on the Southeast
310 U.S. region, using data within the domain of 25 - 40° N latitude and 100 - 75° W longitude
311 for our analyses. A map of all the flight tracks of each campaign is shown in Figure S4. All
312 model results are sampled along the flight track with 1-min time resolution.

313 **4.1 Mean vertical profiles of O₃ and RON**

314 Figure 1 shows the observed and modeled mean vertical profiles of O₃, NO_x, HNO₃, PAN,
315 Σ ANs and NO_y during ICARTT and SENEX. We use Σ ANs measurements from
316 SEAC⁴RS to evaluate model performance during summer 2013, due to the lack of Σ ANs
317 measurements from SENEX. Our model results include both gas and aerosol RONO₂ in
318 Σ ANs, although aerosol RONO₂ accounts for 7~11% of Σ ANs in the planetary boundary
319 layer (PBL, < 1.5 km). We do not consider inorganic nitrates in particle phase in this
320 analysis, due to lack of thermodynamic model for inorganic aerosols in current version of
321 AM3. This simplification is expected to have minimal effects, as they only account for a
322 small fraction of aerosol nitrates in the Southeast U.S. (Ng et al., 2017). To investigate the
323 impact of RONO₂ hydrolysis, we include two model simulations, the base case with
324 heterogeneous loss of ISOPNB, and a sensitivity run ‘no_hydro’ without heterogeneous
325 loss of organic nitrates.

326 Mean observed O₃ in the surface layer decreased from 50 ppb during ICARTT to 35 ppb
327 during SENEX, consistent with the declining trend in surface MDA8 ozone at AQS
328 monitoring sites (section 5.2). As we show in section 5.2, this decline in ozone is mainly
329 driven by NO_x emission reduction, with little influence by meteorology in the two years.
330 Our model can reproduce the vertical gradient and the relative change of O₃ from 2004 to
331 2013, except for a positive absolute bias of 6 - 12 ppb in the boundary layer. Performance
332 statistics of O₃ in the boundary layer listed in Table S4 also indicate positive biases in the
333 model, with the fractional bias (FB) of 9.4 – 17%, fractional error (FE) of 16 – 19 %,
334 normalized mean bias (NMB) of 9.4 – 16% and normalized mean error (NME) of 16 –
335 19 %. This overestimate of O₃ is higher than that reported (3 - 5 ppb) by Mao et al. (2013b)
336 for their simulation of the ICARTT dataset, likely due to faster photolysis of carbonyl
337 nitrates that increases the NO_x recycling efficiency from isoprene oxidation.

338 We further examine mean vertical profiles of NO_x and its reservoirs in 2004 and 2013
339 (Figure 1). In the boundary layer along the flight tracks, HNO₃ is the most abundant RON,
340 accounting for 40 - 46 % of NO_y, followed by NO_x (18 - 23 %), PAN (20 %), and Σ ANs
341 (11 - 21 %). Between 2004 and 2013, mean observed NO_y in the boundary layer decreased
342 by 20 %, from 2.0 ppb to 1.6 ppb, a weaker change than the 35 % reduction of total NO_x
343 emissions (Table 1). The responses of major RON are mostly proportional to the change in
344 NO_x emissions, with the notable exception of Σ ANs. We find significant decreases in NO_x
345 (- 35 %) and HNO₃ (- 29 %) as well as a slight decrease in PAN (- 13 %) from observations.

346 The relative trends of HNO₃ and PAN are opposite to those found in the Los Angeles (LA)
347 basin, where PAN decreased much faster than HNO₃ (Pollack et al., 2013). This difference
348 results mainly from the rapid decrease of anthropogenic VOC emissions in the LA basin
349 that also serves as major precursors of PAN. In contrast, isoprene is the major precursor of
350 PAN over the Southeast U.S. Its emissions show a constant supply (within 5 % differences
351 over the two summers) in this region. Σ ANs shows a different trend from the above
352 compounds, increasing from 0.23 ppb to 0.27 ppb (+ 17 %) near the surface. As we show
353 below in section 5.1, these changes (except for Σ ANs) are mostly consistent with model
354 estimates on a regional average. Discrepancy in their trends of vertical profiles and regional
355 average might be due to representative errors from the three aircraft campaigns on spatial
356 (Figure S4) and temporal (different episodes, referring to observation data description in
357 section 3) scales.

358 The model can well reproduce RON in the boundary layer but tend to underestimate them
359 in the free troposphere. This is likely due to insufficient production of NO_x from lightning
360 in the free troposphere in our model, which is 0.048 Tg N in total over North America
361 during July - August of 2004, lower by almost a factor of 5 compared to the value (0.27 Tg
362 N from July 1-August 15, 2004) reported by Hudman et al. (2007). This underestimate can
363 be improved by scaling up lightning emission by a factor of 5-10 (Fang et al., 2010). We
364 do not adjust the lightning NO_x emissions in this work due to its high uncertainty (Ott et
365 al., 2010; Pickering et al., 1998).

366 Hydrolysis of organic nitrates affects RONO₂ significantly in the boundary layer. By
367 introducing hydrolysis of ISOPNB, we find that model relative bias of Σ ANs is reduced
368 from + 20 % to + 2 % during ICARTT (Figure 1). Performance metrics in Table S4 also
369 indicate better agreement of the model with observations if hydrolysis of ISOPNB assumed.
370 However, the relative bias is increased in magnitude from - 9 % to - 24 % during SEAC⁴RS.
371 This low bias can be partially due to neglecting small alkyl nitrates, which could contribute
372 20 - 30 ppt to Σ ANs (less than 10% near the surface) during SEAC⁴RS (Fisher et al., 2016).
373 Including small alkyl nitrates will increase modeled Σ ANs a bit in ICARTT as well.
374 Hydrolysis of ISOPNB also leads to a slight increase of HNO₃ (Table S4). The impact of
375 hydrolysis of ISOPNB on boundary layer O₃ appears to be small. This is mainly because
376 without hydrolysis, the dominant loss of ISOPNB is oxidation by OH, which then leads to
377 the formation of secondary organic nitrates including MVKN, MACRN and DHDN. The
378 majority of these organic nitrates (MVKN and DHDN) return NO_x slowly due to their long
379 lifetimes (Table S5), resulting in a similar effect on ozone production as hydrolysis of
380 ISOPNB. In addition to the good agreement of Σ ANs, our model shows good agreement
381 with speciated RONO₂ measured during SENEX and SEAC⁴RS, including ISOPN and the
382 sum of MVKN and MACRN (Figure 2). We find that the large discrepancy between Σ ANs
383 and speciated alkyl nitrates (Figure S5) can be explained by a combination of monoterpene

384 nitrates and DHDN and nighttime NO₃ oxidation products from isoprene, accounting for
385 20 - 24 %, 14 - 17 % and 23 - 29 % of Σ ANs respectively in the boundary layer.

386 Given the good agreement between observed and modeled RON in both 2004 and 2013,
387 we find that the ozone bias, shown in Figure 1, cannot be completely explained by an
388 overestimate of anthropogenic NO_x emissions. A recent GEOS-Chem study (Travis et al.,
389 2016) shows that the ozone bias in their model can be largely reduced by scaling down
390 anthropogenic NO_x emissions. We find that a similar reduction of anthropogenic NO_x
391 emissions in 2013, from 0.25 Tg N mon⁻¹ to 0.15 Tg N mon⁻¹, would lead to an
392 underestimate of NO_y, HNO₃ and PAN by 30 %, 33 % and 30 %, respectively. Such a
393 reduction would be also inconsistent with the relative changes in EPA estimates of NO_x
394 emissions shown above. Indeed, other processes, such as ozone dry deposition, may also
395 contribute to this bias and warrant further investigation.

396 **4.2 NO₃⁻ wet deposition flux and concentration**

397 Figure 3 shows a comparison of NO₃⁻ wet deposition flux between observations and model
398 results during the summers of 2004 and 2013. The observed NO₃⁻ wet deposition flux is
399 calculated by multiplying the measured NO₃⁻ concentration and precipitation at each
400 monitoring site as $F_{o,i}=C_{o,i}P_{o,i}$, where $F_{o,i}$ is the monthly-mean NO₃⁻ wet deposition flux,
401 $C_{o,i}$ and $P_{o,i}$ are the monthly-mean observed NO₃⁻ concentration precipitation at monitoring
402 site i . The modeled NO₃⁻ wet deposition flux includes HNO₃ and all the alkyl nitrates.
403 Observations indicate a 24 % reduction of NO₃⁻ wet deposition flux in summer from 2004
404 to 2013 over the Southeast U.S., likely due to NO_x emission reductions. This reduction in
405 monthly averaged NO₃⁻ wet deposition flux is well captured by our model (-29 %), despite
406 a low relative bias of 40 % in both years and NMB of - 39 – - 43 % (Table S4).

407 Since errors in modeled precipitation could strongly affect the modeled NO₃⁻ wet deposition
408 flux (Appel et al., 2011; Grimm and Lynch, 2005; Metcalfe et al., 2005; Paulot et al., 2014;
409 Tost et al., 2007), we also evaluate the modeled NO₃⁻ concentration ($C_{p,i}$), which is
410 calculated by using the modeled NO₃⁻ wet deposition flux ($F_{p,i}$) and observed precipitation
411 ($P_{o,i}$; $C_{p,i}=F_{p,i}/P_{o,i}$), as a separate constraint. The model shows a similar declining trend
412 from the observations with a relative bias of - 23 % and - 41 % on NO₃⁻ concentration for
413 2004 and 2013 respectively. Our results are consistent with the base case of Paulot et al.
414 (2016), which showed that convective removal is likely insufficient in AM3, leading to
415 underestimates of both NO₃⁻ wet deposition flux and concentrations. Our results are
416 somewhat different from a recent GEOS-Chem study (Travis et al., 2016). They found that
417 reducing anthropogenic NO_x emissions from NEI11v1 by 53 % can significantly improve
418 the overestimate of 71 % on NO₃⁻ wet deposition flux in their model during August-
419 September of 2013. A further reduction of anthropogenic NO_x emissions in our model (to

420 0.15 Tg N mon⁻¹), as suggested by Travis et al. (2016), would lead to an even greater
421 negative bias compared to observations.

422 4.3 RONO₂ and related species

423 We further evaluate RONO₂ and related species in this section, with a large focus on
424 measurements from ICARTT and SEAC⁴RS. The major pathway for the production of
425 daytime RONO₂ is the reaction of NO with RO₂ originating from VOC oxidation by OH:



426 where α is the branching ratio for alkyl nitrate formation. NO₂ subsequently undergoes
427 photolysis to produce O₃:



428 For isoprene, α is 9 ± 4 % (for ISOPN) according to a recent study (Xiong et al., 2015).
429 For monoterpenes, specifically α -pinene, α ranges from 1 % to 26 % (Rindelaub et al.,
430 2015; Nozière et al., 1999; Aschmann et al., 2002). Here, we use 10 % for isoprene and
431 26 % for monoterpenes. As RONO₂ and O₃ are both produced from (R4), a correlation
432 between them is expected. We show that the model can roughly reproduce the correlation
433 of O_x (= O₃ + NO₂) vs. Σ ANs during both ICARTT and SEAC⁴RS (Figure 4), although the
434 slope has a positive relative bias of about 21 % and 33 % respectively, largely due to an
435 overestimate of O₃ in the model. The good agreement between observed and modeled O_x
436 vs. daytime RONO₂ provides additional support for our treatment of the yields and fate of
437 these daytime isoprene nitrates.

438 Another metric to evaluate RONO₂ chemistry is the correlation between Σ ANs and HCHO,
439 as the latter is a coproduct from (R4). We show in Figure 4 that the model can roughly
440 capture the observed Σ ANs-HCHO slope, with an underestimate by 25 % and 13 % during
441 ICARTT and SEAC⁴RS, respectively. The underestimate is in part due to small alkyl
442 nitrates that are neglected in the model, as mentioned in section 4.1. During ICARTT, the
443 slope estimated by AM3 is 0.12, similar to the value (0.15) from a previous GEOS-Chem
444 study using a different isoprene oxidation mechanism that assumed a higher α (of 4.7%
445 from ISOPNB and 7.0% from ISOPND vs. 10 % of ISOPNB and zero ISOPND in AM3)
446 and a lower yield of HCHO (66 % vs. 90 % in AM3) (Mao et al., 2013b). The reason for
447 such similarity between the two models might be two-fold: (a) the additional contribution
448 of monoterpene nitrates to Σ ANs in AM3 compensates for the decrease in α from isoprene
449 nitrates compared to GEOS-Chem and (b) the coarse grid resolution of GEOS-Chem

450 simulation ($2^\circ \times 2.5^\circ$) may lead to a higher estimate of HCHO compared to the result from
451 a finer grid resolution (Yu et al., 2016).

452 Since HCHO can be produced from other pathways of isoprene hydroxyl peroxy radicals
453 (ISOPO₂) besides (R4) (such as isomerization of ISOPO₂ and ISOPO₂ + HO₂), changes in
454 the slope of Σ ANs vs. HCHO may help to quantify decadal changes in isoprene oxidation
455 pathways. We find in Figure 4 that the observed slope of Σ ANs-HCHO shows very little
456 change from 2004 to 2013. This is in part due to substantial HCHO production from
457 isoprene oxidation under low NO_x conditions (Li et al., 2016), and in part due to the
458 buffering of Σ ANs in response to decreasing NO_x, as shown below in section 5.1. Our
459 model is able to reproduce such behavior. We also find that the branching ratios for the
460 reactions of ISOPO₂ change marginally from 2004 to 2013 over the Southeast U.S. (Figure
461 S6). The fraction of ISOPO₂ + NO has decreased from 81 % in 2004 to 66 % in 2013. The
462 fraction of ISOPO₂ + HO₂ has increased from 15 % to 28 %, and the fraction of ISOPO₂
463 isomerization has increased from 4 % to 6 %. Our result is slightly different from the results
464 of GEOS-Chem, which found a lower contribution from the NO pathway (54 %) and higher
465 from isomerization (15 %) during August - September of 2013 (Travis et al., 2016).

466 We also compare the correlation between major daytime isoprene nitrates and HCHO
467 during 2013, which provides a constraint on the yield of these nitrates. Our model shows a
468 slight overestimate on the slope (Figure 4 (b)), consistent with comparison of mean vertical
469 profiles shown in Figure 2. The computed slope (5 %) in this study is different from that
470 (2.5 %) of a recent GEOS-Chem simulation by Fisher et al. (2016). This is partially due to
471 the different treatment of β - and δ -ISOPO₂ between GEOS-Chem and AM3. Another factor
472 is that MVKN and MACRN are not allowed to hydrolyze in AM3, leading to higher
473 abundance of these two nitrates.

474 Figure 5 shows the mean vertical profiles of modeled monoterpene nitrates (MNs) and
475 isoprene nitrates (INs) during ICARTT and SEAC⁴RS. INs are the most abundant RONO₂,
476 accounting for 76-80 % below 3 km over the Southeast U.S. In the measurements, ISOPN
477 + MVKN + MACRN only contribute one third of the total INs (Figure S5). We show below
478 that the discrepancy of Σ ANs and speciated RONO₂ can be explained by other daytime and
479 nighttime INs as well as MNs in the model. More than 60 % of modeled INs originate from
480 isoprene oxidation during daytime. The first-generation nitrate ISOPN contributes slightly
481 more (31 %) than the second-generation nitrates MVKN + MACRN (28 %) to the total
482 daytime INs during ICARTT. This is different from Mao et al. (2013b) who showed a
483 higher contribution of MVKN + MACRN than the first-generation INs, due to the different
484 treatment of β - and δ -ISOPO₂. We see more ISOPN (32 %) than MVKN + MACRN (26 %)
485 from the daytime INs during SEAC⁴RS, consistent with Fisher et al. (2016). A large
486 uncertainty in our model is attributed to DHDN, which contributes 32 % to the daytime
487 INs. Fisher et al. (2016) showed less DHDN during SEAC⁴RS since it was removed rapidly

488 by hydrolysis (1-h lifetime) in their model. Our sensitivity test (hydro_full, Figure S2)
489 indicates that AM3 would significantly underestimate Σ ANs if we assume a similar
490 heterogeneous loss of DHDN as ISOPN. In fact, DHDN was hypothesized originally in
491 Lee et al. (2014) for the imbalance of nitrogen in their lab experiments, and may serve as
492 a proxy for a large number of unidentified daytime INs. It remains unclear what the
493 dominant loss of DHDN is. Daytime nitrates from monoterpene oxidation are another
494 important source of Σ ANs in this region, accounting for 17 - 20 % (24 - 26 ppt) of the total.
495 Fisher et al. (2016) estimate a smaller burden of MNs, of about 10 - 20 ppt due to a lower
496 molar yield (18 % vs. 26 % in AM3) and faster hydrolysis of MNs in their model.

497 Nighttime chemistry contributes about 30 - 36 % of Σ ANs, which is dominated by isoprene
498 oxidation as well (Figure 5). 33 - 41 % of the INs are produced during night, similar to the
499 value (44 %) reported by Mao et al. (2013b) but with different speciation, due to the
500 different treatment of chemistry. PROPNN contributes about 29-38 % of the total INs.
501 PROPNN in this work is mainly produced from the oxidation of C5 nitrooxy hydroperoxide
502 (INPN) and C5 carbonyl nitrate (ISN1; dominantly by photolysis) that are generated from
503 isoprene oxidation by NO_3 during the nighttime. This is different from Fisher et al. (2016),
504 who showed that PROPNN is partially from the δ -ISOPO₂ + NO pathway and partially
505 from the oxidation of ISN1 by NO_3 . In our model, we see a rapid increase of PROPNN
506 after sunrise in the boundary layer (Figure S7), consistent with observations at the Southern
507 Oxidants and Aerosols Study (SOAS) ground site CTL (Schwantes et al., 2015). Our model
508 overestimates the mean vertical profile of PROPNN by a factor of 3 (not shown). As our
509 model may largely underrepresent the chemical complexity of nighttime isoprene oxidation
510 as shown by Schwantes et al. (2015), we consider PROPNN as a proxy for other
511 unspecified isoprene nighttime nitrates. Over all, PROPNN contributes a significant
512 fraction of Σ ANs in the model, 23 - 29 % in the boundary layer as shown in section 4.1.
513 With monoterpene nitrates and isoprene derived DHDN and nighttime NO_3 oxidation
514 products taken into account, we find that model can well reproduce both observed Σ ANs
515 and speciated alkyl nitrates (Figure S5).

516 **5 Decadal Change of PBL RON and surface ozone over SEUS**

517 As RON and related species from aircraft and surface measurements are well reproduced
518 in our model for both 2004 and 2013, we assume that the model is representative of this
519 chemical environment, and then use the model to derive monthly mean changes between
520 2004 and 2013. We also investigate the impacts of further decreases in NO_x emissions by
521 applying a hypothetical 40 % reduction of anthropogenic NO_x emissions of 2013 but
522 keeping other emissions and meteorology the same (“hypo” case in Table 2).

523 **5.1 RON**

524 We first examine the simulated decadal change of RON in the boundary layer over the
525 Southeast U.S. as shown in Figure 6. In summer of 2004, the model suggests that NO_y is
526 mainly comprised of HNO_3 (45 %), NO_x (31 %), ΣPNs (14 %) and ΣANs (9 %). In
527 response to a 40 % reduction in anthropogenic NO_x emissions (35 % reduction in total NO_x
528 emissions, Table 1) from 2004 to 2013, NO_y declined by 34 %. This modeled response is
529 comparable to long-term NO_y measurements from the AQS surface network, which shows
530 on average a 45 % decrease from 2004 to 2013 over the Southeast U.S. Based on model
531 estimates in Figure 6, most RON are reduced proportionally, with decreases of 38 % for
532 HNO_3 , 32 % for NO_x and 34% for ΣPNs . The different change in ΣPNs and PAN (the
533 majority of ΣPNs) in Figure 1 might be due to the difference in sampling regions. The only
534 exception is ΣANs , with a smaller decline of 19 %. As an important source of organic
535 aerosols (OA), ΣANs may contribute to the decrease of OA over the Southeast U.S. in the
536 past decade (Blanchard et al., 2016).

537 We conducted a sensitivity test with an additional 40 % reduction of anthropogenic NO_x
538 emissions from 2013. We find that NO_y decreases by 29 %, with a proportional decrease
539 in HNO_3 , NO_x , and ΣPNs (Figure 6). The slower decrease of NO_y is likely due to ΣANs ,
540 which decrease at a slower rate and becomes a larger fraction of NO_y . The buffering of
541 ΣANs is consistent with previous studies (Browne and Cohen, 2012; Fisher et al., 2016),
542 mainly due to lower OH resulting from decreased NO_x (Figure S8) and thus a prolonged
543 lifetimes of NO_x and ΣANs (Browne and Cohen, 2012). As shown in Figure S8, averaged
544 noontime OH decreases by 11 % from 2004 to 2013 and by 29 % after we impose an
545 additional 40 % NO_x emission reduction from 2013 levels.

546 The historical NO_x emission reduction also affects reactive nitrogen export out of the
547 boundary layer. Here we define exported nitrogen as the difference of the sources
548 (chemical production and emissions) and sinks (chemical loss, wet and dry deposition). As
549 shown in Table 3, total summertime NO_y export from the Southeast U.S. boundary layer
550 decreases proportionally, from 24.1 Gg N in 2004 to 16.6 Gg N in 2013. The NO_y export
551 efficiency, calculated as net exported nitrogen divided by total NO_x emissions, remains
552 roughly the same (12 %) for 2004 and 2013, comparable to previous studies (Fang et al.,
553 2010; Li et al., 2004; Parrish et al., 2004; Mao et al., 2013b; Sanderson et al., 2008;
554 Hudman et al., 2007). Among all exported species, NO_x contributes most of net export
555 from the PBL (6 % of total NO_x emissions), followed by PAN (4 %) and ΣANs (2 %). We
556 emphasize in Table 3 that a major fraction of NO_x is exported through the top of the
557 boundary layer (convection). From a budget calculation throughout the tropospheric
558 column over the same region, we find that despite being the same NO_y export efficiency
559 (12 %), HNO_3 becomes the major exporter, accounting for half of NO_y export efficiency
560 from the total column (6 %). The contributions from PAN and ΣANs are roughly the same
561 as their export from the boundary layer (4 % and 2 %). This suggests that surface
562 NO_x ventilated through the boundary layer, converted to HNO_3 in the free troposphere and

563 exported as HNO₃ is likely the major NO_y export mechanism over the Southeast U.S. in
564 our model, which is in agreement with previous observations (Parrish et al., 2004; Neuman
565 et al., 2006). PAN and ΣANs together account for another half of NO_y export efficiency.
566 As PAN and ΣANs are of biogenic origin and longer lived than HNO₃, they may play a
567 key role in influencing RON and ozone in downwind regions (Moxim et al., 1996; Fischer
568 et al., 2014).

569 **5.2 Surface ozone**

570 Since the mid-1990s, NO_x emission controls have led to significant improvement on ozone
571 air quality over the eastern U.S. (Simon et al., 2015; Cooper et al., 2012). As NO_x emissions
572 continue to decrease, ozone production efficiency (OPE) may increase due to the lower
573 NO_x removal rate by OH and to some extent may compensate the ozone reduction (Sillman,
574 2000). Meanwhile, surface ozone production may be further complicated by the increasing
575 importance of RO₂ isomerization and RO₂ + HO₂. Here we first evaluate our model against
576 surface ozone observations in 2004 and 2013, and then project the future response of
577 surface ozone to even lower NO_x emissions to examine the efficacy of near-term NO_x
578 emission controls at lowering near-surface ozone levels.

579 We first examine the modeled surface ozone against observations at 157 EPA AQS
580 monitoring sites over the Southeast U.S. in July-August of 2004 and 2013 (Figure S9). In
581 general, AM3 overestimates surface MDA8 ozone in both years by about 16 ppb on
582 average, with the NMB of 33 - 45 % and NME of 35 - 46 % respectively. This positive
583 bias of summertime surface O₃ has been a common issue to a number of modeling studies
584 of this region (Fiore et al., 2009; Canty et al., 2015; Brown-Steiner et al., 2015; Strode et
585 al., 2015; Travis et al., 2016). This might be partially attributed to overestimated
586 anthropogenic NO_x emissions from non-power plant sectors, excessive vertical mixing in
587 the boundary layer (Travis et al., 2016) or underestimates of O₃ dry deposition (Hardacre
588 et al., 2015; Val Martin et al., 2014). Further studies are warranted to investigate the cause
589 of this bias in AM3.

590 Surface O₃ concentrations over the Southeast U.S. decline substantially from 2004 to 2013
591 in response to the large NO_x emission reduction (Simon et al., 2015). MDA8 ozone
592 averaged across all the monitoring sites is observed to decrease by 11 ppb (23 % of
593 observed mean MDA8 ozone in July-August of 2004) resulting from approximately 40 %
594 reductions of anthropogenic NO_x emissions (35 % reduction in total NO_x emissions). This
595 strong sensitivity of surface ozone to NO_x emission reflects the linear relationship between
596 ozone production rate and NO_x concentrations when NO_x is low (Trainer et al., 2000). Our
597 model is able to capture this strong NO_x - O₃ sensitivity, with the mean MDA8 ozone
598 reduced by 10 ppb from 2004 to 2013. We find that a further 40 % reduction of
599 anthropogenic NO_x emissions with identical meteorological conditions could lead to an
600 additional 9 ppb decrease, a similar magnitude to the change from 2004 to 2013.

601 We further investigate the impact of temperature and moisture on surface O₃ from 2004 to
602 2013. While several studies suggest that surface O₃ increases with ambient temperature
603 (Jacob and Winner, 2009; Bloomer et al., 2010; Wu et al., 2008; Steiner et al., 2010),
604 Cooper et al. (2012) showed that this temperature related impact is weak during the period
605 of 1990-2010 across the U.S.A. Recent studies suggest that relative humidity (RH) or vapor
606 pressure deficit (VPD) may play an important role in ozone variability through soil-
607 atmosphere or biosphere-atmosphere coupling (Kavassalis and Murphy, 2017; Camalier et
608 al., 2007; Tawfik and Steiner, 2013). Our model shows marginal differences in RH (less
609 than 1 %) and temperature (+ 2.4 K) within the PBL over the Southeast U.S. between the
610 summers of 2004 and 2013, consistent with observed changes of RH (+ 2.7 %) and
611 temperature (+ 2.6 K) during ICARTT and SENEX. This small variation in the model is
612 also consistent with climatology data (Hidy et al., 2014). Camalier et al. (2007) showed
613 that RH has a much bigger impact on summertime ozone than temperature over the
614 Southeast U.S., suggesting little influence of meteorology on ozone trend. Using the same
615 model but with the standard AM3 chemical mechanism, Lin et al. (2017) found that
616 meteorology changes would have caused high surface ozone over the eastern U.S. to
617 increase by 0.2 - 0.4 ppb yr⁻¹ in the absence of emission controls from 1988 to 2014.
618 Therefore, we conclude that the impact of climate variability and change on O₃ is relatively
619 small compared to NO_x emission reductions over the Southeast U.S., consistent with
620 previous studies (Lam et al., 2011; Hidy et al., 2014; Lin et al., 2017; Rieder et al., 2015).

621 Decreasing NO_x emissions also reduces the frequency of high O₃ pollution events. Figure
622 7 shows the probability density function of observed and modeled MDA8 ozone at each
623 monitoring site during July-August of 2004 and 2013, and the probability density function
624 of modeled MDA8 ozone under a hypothetical scenario with another 40 % reduction in
625 anthropogenic NO_x emissions compared to 2013. We show that the lowest O₃, about 20
626 ppb in current model simulations, remains invariant with NO_x emission changes over the
627 Southeast U.S., consistent with observations (Figure 7 (a)). Meanwhile, the high tail of
628 MDA8 ozone events has shifted from more than 100 ppb in 2004 to about 85 ppb after the
629 40 % reduction of anthropogenic NO_x emissions from 2013. A similar shift is found in
630 observations. The narrowing of the range of O₃ with decreasing NO_x is consistent with the
631 observed trends reported by Simon et al. (2015). We also find that further reductions of
632 NO_x emissions will reduce both median O₃ values and the high tail, suggesting that fewer
633 high ozone events will occur under continued NO_x emission controls in the future.

634 **6 Conclusions and Discussions**

635 Near-surface ozone production over the Southeast U.S. is heavily influenced by both
636 anthropogenic and biogenic emissions. We investigate the response of NO_y speciation to
637 the significant NO_x emission controls (about 40 % reduction) in this region over the past
638 decade, in light of the fast-evolving understanding of isoprene photooxidation. This
639 knowledge is needed to predict nitrogen and ozone budgets in this region and elsewhere in

640 the world with similar photochemical environments. Here we use extensive aircraft and
641 ground observations, combined with a global chemistry-climate model (GFDL AM3), to
642 examine decadal changes in NO_y abundance and speciation as well as in surface O_3 mixing
643 ratios over the Southeast U.S. between the summers of 2004 and 2013. We then use the
644 model to infer future NO_y speciation and surface ozone abundances in response to further
645 NO_x emission controls in this region.

646 We first evaluate the model with aircraft and surface observations. When we apply the
647 estimated 40 % reductions in anthropogenic NO_x emissions from 2004 to 2013, our model
648 reproduces the major features of vertical profiles of NO_x , HNO_3 , PAN, ΣANs and NO_y
649 observed during aircraft campaigns over the Southeast U.S. in the summers of 2004 and
650 2013. By including recent updates to isoprene oxidation, our model can largely reproduce
651 the vertical profiles of ΣANs and several speciated alkyl nitrates, as well as their
652 correlations with O_x and HCHO, lending support to the model representation of isoprene
653 oxidation. On the other hand, we show that a discrepancy between measured ΣANs and
654 speciated RONO_2 can be explained by a combination of monoterpene nitrates, dinitrates
655 and nighttime NO_3 oxidation products from isoprene. We also show that modeled ozone
656 appears to be insensitive to hydrolysis of ISOPNB, because its photooxidation, mainly by
657 OH, also returns little NO_x .

658 Major RON decline proportionally as a result of NO_x emission reductions in the Southeast
659 U.S., except for a slower rate in ΣANs . The slower decline of ΣANs reflects the prolonged
660 lifetime of NO_x when it is decreasing. Our model suggests that summertime monthly
661 averaged NO_x , HNO_3 , PAN, and NO_y decline by 30 - 40 %, in response to 40 % reduction
662 in anthropogenic NO_x emissions from 2004 to 2013. This proportional decrease is likely
663 driven by high concentrations of biogenic VOCs, the major precursor of PAN in this region
664 that change little in magnitude from 2004 to 2013. In contrast, Pollack et al. (2013) find a
665 faster PAN decrease than HNO_3 in the LA basin over the past several decades, partly due
666 to the decrease in anthropogenic VOC emissions that are major PAN precursors.

667 Deposited and exported NO_y decline with NO_x emission reductions. The model also shows
668 a decrease of NO_3^- wet deposition flux by 29 % from 2004 to 2013, consistent with
669 observations from the NADP network (- 24 %). We find from model calculations that the
670 NO_y export efficiency remains at 12 % in both 2004 and 2013, leading to a proportional
671 decrease of exported NO_y . The dominant NO_y export terms include NO_x or HNO_3 , each
672 accounting for 6% of the total exported NO_y , followed by ΣPNs (4 %) and ΣANs (2 %).

673 The response of surface ozone to NO_x emission reductions reveals a strong $\text{NO}_x - \text{O}_3$
674 sensitivity in summertime over the Southeast U.S. Observations from EPA AQS surface
675 network suggest that mean MDA8 ozone during July-August has decreased by 23%, from
676 48 ppb in 2004 to 37 ppb in 2013. Despite a positive absolute bias of up to 12 ppb in

677 boundary layer ozone and 16 ppb in surface MDA8 ozone, our model shows a 10 ppb
678 decrease of surface MDA8 ozone from 2004 to 2013, very close to the observed 11 ppb
679 decrease from the EPA data. The bias of ozone in our model is not entirely attributed to
680 uncertainties in NO_x emissions, as the overestimate suggested by earlier work would lead
681 to an underestimate of NO_y (Travis et al., 2016). Care should be exercised in applying the
682 modeling results for surface ozone regulation purposes, given the high ozone bias shown
683 in our model. We find from model calculations that modeled MDA8 O₃ will continue to
684 decrease by another 9 ppb assuming anthropogenic NO_x emissions are reduced by 40 %
685 from 2013 levels with meteorology and other emissions kept the same. In addition, further
686 NO_x emission reduction leads to less frequent high ozone events. This continued strong
687 sensitivity of surface O₃ to NO_x emissions can guide the development of effective emission
688 control strategies for improving future air quality.

689 **Data availability**

690 Observational datasets and modeling results are available upon request to the
691 corresponding author (jmao2@alaska.edu).

692 **Competing interests**

693 The authors declare that they have no conflict of interest.

694 **Acknowledgements**

695 The authors thank Vaishali Naik (NOAA GFDL) for providing emission inventories in the
696 GFDL AM3 model, and Leo Donner (NOAA GFDL) and William Cooke (UCAR/NOAA)
697 for the help with convection scheme of AM3. J.L., J.M. and L.W.H. acknowledge support
698 from the NOAA Climate Program Office grant # NA13OAR431007. J.M., L.W.H. and
699 A.M.F. acknowledge support from NOAA Climate Program Office grant
700 #NA14OAR4310133. J.D.C. and P.O.W. acknowledge support from NASA grants
701 (NNX12AC06G and NNX14AP46G). J.L. acknowledge support from the Startup
702 Foundation for Introducing Talent of NUIST grant #2243141701014 and the Priority
703 Academic Program Development of Jiangsu Higher Education Institutions (PAPD).

704 **References**

- 705 Anderson, D. C., Loughner, C. P., Diskin, G., Weinheimer, A., Canty, T. P., Salawitch,
706 R. J., Worden, H. M., Fried, A., Mikoviny, T., Wisthaler, A., and Dickerson, R. R.:
707 Measured and modeled CO and NO_y in DISCOVER-AQ: An evaluation of emissions
708 and chemistry over the eastern US, *Atmos. Environ.*, 96, 78-87, 2014.
- 709 Appel, K., Foley, K., Bash, J., Pinder, R., Dennis, R., Allen, D., and Pickering, K.: A
710 multi-resolution assessment of the Community Multiscale Air Quality (CMAQ) model
711 v4. 7 wet deposition estimates for 2002–2006, *Geosci. Model. Dev.*, 4, 2, 357-371, 2011.
- 712 Aschmann, S. M., Atkinson, R., and Arey, J.: Products of reaction of OH radicals with α
713 - pinene, *J. Geophys. Res.*, 107, D14, 2002.
- 714 Astitha, M., Luo, H., Rao, S. T., Hogrefe, C., Mathur, R., and Kumar, N.: Dynamic
715 evaluation of two decades of WRF-CMAQ ozone simulations over the contiguous United
716 States, *Atmos. Environ.*, 164, Supplement C, 102-116, 2017.
- 717 Ayres, B. R., Allen, H. M., Draper, D. C., Brown, S. S., Wild, R. J., Jimenez, J. L., Day,
718 D. A., Campuzano-Jost, P., Hu, W., de Gouw, J., Koss, A., Cohen, R. C., Duffey, K. C.,
719 Romer, P., Baumann, K., Edgerton, E., Takahama, S., Thornton, J. A., Lee, B. H., Lopez-
720 Hilfiker, F. D., Mohr, C., Wennberg, P. O., Nguyen, T. B., Teng, A., Goldstein, A. H.,
721 Olson, K., and Fry, J. L.: Organic nitrate aerosol formation via NO₃ + biogenic volatile
722 organic compounds in the southeastern United States, *Atmos. Chem. Phys.*, 15, 23,
723 13377-13392, 2015.
- 724 Baker, K. R., and Woody, M. C.: Assessing Model Characterization of Single Source
725 Secondary Pollutant Impacts Using 2013 SENEX Field Study Measurements, *Environ.*
726 *Sci. Technol.*, 51, 7, 3833-3842, 2017.
- 727 Bates, K. H., Crouse, J. D., St. Clair, J. M., Bennett, N. B., Nguyen, T. B., Seinfeld, J.
728 H., Stoltz, B. M., and Wennberg, P. O.: Gas Phase Production and Loss of Isoprene
729 Epoxydiols, *J. Phys. Chem. A*, 118, 7, 1237-1246, 2014.
- 730 Bates, K. H., Nguyen, T. B., Teng, A. P., Crouse, J. D., Kjaergaard, H. G., Stoltz, B. M.,
731 Seinfeld, J. H., and Wennberg, P. O.: Production and Fate of C₄ Dihydroxycarbonyl
732 Compounds from Isoprene Oxidation, *J. Phys. Chem. A*, 120, 1, 106-117, 2016.
- 733 Bean, J. K., and Hildebrandt Ruiz, L.: Gas–particle partitioning and hydrolysis of organic
734 nitrates formed from the oxidation of α -pinene in environmental chamber experiments,
735 *Atmos. Chem. Phys.*, 16, 4, 2175-2184, 2016.
- 736 Blanchard, C. L., Hidy, G. M., Shaw, S., Baumann, K., and Edgerton, E. S.: Effects of
737 emission reductions on organic aerosol in the southeastern United States, *Atmos. Chem.*
738 *Phys.*, 16, 1, 215-238, 2016.

739 Bloomer, B. J., Vinnikov, K. Y., and Dickerson, R. R.: Changes in seasonal and diurnal
740 cycles of ozone and temperature in the eastern U.S, *Atmos. Environ.*, 44, 21–22, 2543-
741 2551, 2010.

742 Boyd, C. M., Sanchez, J., Xu, L., Eugene, A. J., Nah, T., Tuet, W. Y., Guzman, M. I., and
743 Ng, N. L.: Secondary organic aerosol formation from the β -pinene+NO₃ system: effect of
744 humidity and peroxy radical fate, *Atmos. Chem. Phys.*, 15, 13, 7497-7522, 2015.

745 Brown-Steiner, B., Hess, P. G., and Lin, M. Y.: On the capabilities and limitations of
746 GCCM simulations of summertime regional air quality: A diagnostic analysis of ozone
747 and temperature simulations in the US using CESM CAM-Chem, *Atmos. Environ.*, 101,
748 134-148, 2015.

749 Browne, E. C., and Cohen, R. C.: Effects of biogenic nitrate chemistry on the NO_x
750 lifetime in remote continental regions, *Atmos. Chem. Phys.*, 12, 24, 11917-11932, 2012.

751 Browne, E. C., Wooldridge, P. J., Min, K. E., and Cohen, R. C.: On the role of
752 monoterpene chemistry in the remote continental boundary layer, *Atmos. Chem. Phys.*,
753 14, 3, 1225-1238, 2014.

754 Camalier, L., Cox, W., and Dolwick, P.: The effects of meteorology on ozone in urban
755 areas and their use in assessing ozone trends, *Atmos. Environ.*, 41, 33, 7127-7137, 2007.

756 Canty, T. P., Hemberck, L., Vinciguerra, T. P., Anderson, D. C., Goldberg, D. L.,
757 Carpenter, S. F., Allen, D. J., Loughner, C. P., Salawitch, R. J., and Dickerson, R. R.:
758 Ozone and NO_x chemistry in the eastern US: evaluation of CMAQ/CB05 with satellite
759 (OMI) data, *Atmos. Chem. Phys.*, 15, 4, 4427-4461, 2015.

760 Cooper, O. R., Gao, R.-S., Tarasick, D., Leblanc, T., and Sweeney, C.: Long-term ozone
761 trends at rural ozone monitoring sites across the United States, 1990–2010, *J. Geophys.*
762 *Res.*, 117, D22307, 2012.

763 Crouse, J. D., Paulot, F., Kjaergaard, H. G., and Wennberg, P. O.: Peroxy radical
764 isomerization in the oxidation of isoprene, *Phys. Chem. Chem. Phys.*, 13, 30, 13607-
765 13613, 2011.

766 Darer, A. I., Cole-Filipiak, N. C., O'Connor, A. E., and Elrod, M. J.: Formation and
767 Stability of Atmospherically Relevant Isoprene-Derived Organosulfates and
768 Organonitrates, *Environ. Sci. Technol.*, 45, 5, 1895-1902, 2011.

769 Donner, L. J., Wyman, B. L., Hemler, R. S., Horowitz, L. W., Ming, Y., Zhao, M., Golaz,
770 J.-C., Ginoux, P., Lin, S.-J., Schwarzkopf, M. D., Austin, J., Alaka, G., Cooke, W. F.,
771 Delworth, T. L., Freidenreich, S. M., Gordon, C. T., Griffies, S. M., Held, I. M., Hurlin,
772 W. J., Klein, S. A., Knutson, T. R., Langenhorst, A. R., Lee, H.-C., Lin, Y., Magi, B. I.,
773 Malyshev, S. L., Milly, P. C. D., Naik, V., Nath, M. J., Pincus, R., Ploshay, J. J.,
774 Ramaswamy, V., Seman, C. J., Shevliakova, E., Sirutis, J. J., Stern, W. F., Stouffer, R. J.,
775 Wilson, R. J., Winton, M., Wittenberg, A. T., and Zeng, F.: The Dynamical Core,
776 Physical Parameterizations, and Basic Simulation Characteristics of the Atmospheric

777 Component AM3 of the GFDL Global Coupled Model CM3, *J. Climate*, 24, 13, 3484-
778 3519, 2011.

779 Edwards, P. M., Aikin, K. C., Dube, W. P., Fry, J. L., Gilman, J. B., de Gouw, J. A.,
780 Graus, M. G., Hanisco, T. F., Holloway, J., Hubler, G., Kaiser, J., Keutsch, F. N., Lerner,
781 B. M., Neuman, J. A., Parrish, D. D., Peischl, J., Pollack, I. B., Ravishankara, A. R.,
782 Roberts, J. M., Ryerson, T. B., Trainer, M., Veres, P. R., Wolfe, G. M., Warneke, C., and
783 Brown, S. S.: Transition from high- to low-NO_x control of night-time oxidation in the
784 southeastern US, *Nature Geosci*, 10, 7, 490-495, 2017.

785 Fang, Y., Fiore, A. M., Horowitz, L., Levy, H., Hu, Y., and Russell, A.: Sensitivity of the
786 NO_y budget over the United States to anthropogenic and lightning NO_x in summer, *J.*
787 *Geophys. Res.*, 115, D18, 2010.

788 Fehsenfeld, F. C., Ancellet, G., Bates, T. S., Goldstein, A. H., Hardesty, R. M., Honrath,
789 R., Law, K. S., Lewis, A. C., Leitch, R., McKeen, S., Meagher, J., Parrish, D. D.,
790 Pszenny, A. A. P., Russell, P. B., Schlager, H., Seinfeld, J., Talbot, R., and Zbinden, R.:
791 International Consortium for Atmospheric Research on Transport and Transformation
792 (ICARTT): North America to Europe—Overview of the 2004 summer field study, *J.*
793 *Geophys. Res.*, 111, D23S01, 2006.

794 Fiore, A. M., Horowitz, L. W., Purves, D. W., Levy, H., Evans, M. J., Wang, Y., Li, Q.,
795 and Yantosca, R. M.: Evaluating the contribution of changes in isoprene emissions to
796 surface ozone trends over the eastern United States, *J. Geophys. Res.*, 110, D12303,
797 2005.

798 Fiore, A. M., Dentener, F. J., Wild, O., Cuvelier, C., Schultz, M. G., Hess, P., Textor, C.,
799 Schulz, M., Doherty, R. M., and Horowitz, L. W.: Multimodel estimates of
800 intercontinental source - receptor relationships for ozone pollution, *J. Geophys. Res.*,
801 114, D4, 83-84, 2009.

802 Fischer, E., Jacob, D. J., Yantosca, R. M., Sulprizio, M. P., Millet, D., Mao, J., Paulot, F.,
803 Singh, H., Roiger, A., and Ries, L.: Atmospheric peroxyacetyl nitrate (PAN): a global
804 budget and source attribution, *Atmos. Chem. Phys.*, 14, 5, 2679-2698, 2014.

805 Fisher, J. A., Jacob, D. J., Travis, K. R., Kim, P. S., Marais, E. A., Miller, C. C., Yu, K.,
806 Zhu, L., Yantosca, R. M., and Sulprizio, M. P.: Organic nitrate chemistry and its
807 implications for nitrogen budgets in an isoprene- and monoterpene-rich atmosphere:
808 constraints from aircraft (SEAC4RS) and ground-based (SOAS) observations in the
809 Southeast US, *Atmos. Chem. Phys.*, 16, 1, 1-38, 2016.

810 Fry, J. L., Kiendler-Scharr, A., Rollins, A. W., Wooldridge, P. J., Brown, S. S., Fuchs,
811 H., Dubé, W., Mensah, A., dal Maso, M., Tillmann, R., Dorn, H. P., Brauers, T., and
812 Cohen, R. C.: Organic nitrate and secondary organic aerosol yield from NO₃ oxidation of
813 β-pinene evaluated using a gas-phase kinetics/aerosol partitioning model, *Atmos. Chem.*
814 *Phys.*, 9, 4, 1431-1449, 2009.

815 Fry, J. L., Draper, D. C., Barsanti, K. C., Smith, J. N., Ortega, J., Winkler, P. M., Lawler,
816 M. J., Brown, S. S., Edwards, P. M., Cohen, R. C., and Lee, L.: Secondary Organic
817 Aerosol Formation and Organic Nitrate Yield from NO₃ Oxidation of Biogenic
818 Hydrocarbons, *Environ. Sci. Technol.*, 48, 20, 11944-11953, 2014.

819 Granier, C., Bessagnet, B., Bond, T., D'Angiola, A., Denier van der Gon, H., Frost, G. J.,
820 Heil, A., Kaiser, J. W., Kinne, S., Klimont, Z., Kloster, S., Lamarque, J.-F., Liousse, C.,
821 Masui, T., Meleux, F., Mieville, A., Ohara, T., Raut, J.-C., Riahi, K., Schultz, M. G.,
822 Smith, S. J., Thompson, A., van Aardenne, J., van der Werf, G. R., and van Vuuren, D.
823 P.: Evolution of anthropogenic and biomass burning emissions of air pollutants at global
824 and regional scales during the 1980–2010 period, *Clim. Change*, 109, 1, 163-190, 2011.

825 Grimm, J. W., and Lynch, J. A.: Improved daily precipitation nitrate and ammonium
826 concentration models for the Chesapeake Bay Watershed, *Environ. Pollut.*, 135, 3, 445-
827 455, 2005.

828 Hardacre, C., Wild, O., and Emberson, L.: An evaluation of ozone dry deposition in
829 global scale chemistry climate models, *Atmos. Chem. Phys.*, 15, 11, 6419-6436, 2015.

830 Henderson, B. H., Pinder, R. W., Crooks, J., Cohen, R. C., Hutzell, W. T., Sarwar, G.,
831 Goliff, W. S., Stockwell, W. R., Fahr, A., Mathur, R., Carlton, A. G., and Vizuete, W.:
832 Evaluation of simulated photochemical partitioning of oxidized nitrogen in the upper
833 troposphere, *Atmos. Chem. Phys.*, 11, 1, 275-291, 2011.

834 Hidy, G. M., Blanchard, C. L., Baumann, K., Edgerton, E., Tanenbaum, S., Shaw, S.,
835 Knipping, E., Tombach, I., Jansen, J., and Walters, J.: Chemical climatology of the
836 southeastern United States, 1999-2013, *Atmos. Chem. Phys.*, 14, 21, 11893-11914, 2014.

837 Hidy, G. M., and Blanchard, C. L.: Precursor reductions and ground-level ozone in the
838 Continental United States, *J. Air Waste Manag. Assoc.*, 65, 10, 1261-1282, 2015.

839 Horowitz, L. W., Liang, J., Gardner, G. M., and Jacob, D. J.: Export of reactive nitrogen
840 from North America during summertime: Sensitivity to hydrocarbon chemistry, *J.*
841 *Geophys. Res.*, 103, D11, 13451-13476, 1998.

842 Horowitz, L. W., Fiore, A. M., Milly, G. P., Cohen, R. C., Perring, A., Wooldridge, P. J.,
843 Hess, P. G., Emmons, L. K., and Lamarque, J.-F.: Observational constraints on the
844 chemistry of isoprene nitrates over the eastern United States, *J. Geophys. Res.*, 112,
845 D12S08, 2007.

846 Hu, K. S., Darer, A. I., and Elrod, M. J.: Thermodynamics and kinetics of the hydrolysis
847 of atmospherically relevant organonitrates and organosulfates, *Atmos. Chem. Phys.*, 11,
848 16, 8307-8320, 2011.

849 Hudman, R., Jacob, D. J., Cooper, O., Evans, M., Heald, C., Park, R., Fehsenfeld, F.,
850 Flocke, F., Holloway, J., and Hübler, G.: Ozone production in transpacific Asian
851 pollution plumes and implications for ozone air quality in California, *J. Geophys. Res.*,
852 109, D23, 2004.

853 Hudman, R. C., Jacob, D. J., Turquety, S., Leibensperger, E. M., Murray, L. T., Wu, S.,
854 Gilliland, A. B., Avery, M., Bertram, T. H., Brune, W., Cohen, R. C., Dibb, J. E., Flocke,
855 F. M., Fried, A., Holloway, J., Neuman, J. A., Orville, R., Perring, A., Ren, X., Sachse,
856 G. W., Singh, H. B., Swanson, A., and Wooldridge, P. J.: Surface and lightning sources
857 of nitrogen oxides over the United States: Magnitudes, chemical evolution, and outflow,
858 *J. Geophys. Res.*, 112, D12S05, 2007.

859 Hudman, R. C., Murray, L. T., Jacob, D. J., Turquety, S., Wu, S., Millet, D. B., Avery,
860 M., Goldstein, A. H., and Holloway, J.: North American influence on tropospheric ozone
861 and the effects of recent emission reductions: Constraints from ICARTT observations, *J.*
862 *Geophys. Res.*, 114, D7, 2009.

863 Hudman, R. C., Moore, N. E., Mebust, A. K., Martin, R. V., Russell, A. R., Valin, L. C.,
864 and Cohen, R. C.: Steps towards a mechanistic model of global soil nitric oxide
865 emissions: implementation and space based-constraints, *Atmos. Chem. Phys.*, 12, 16,
866 7779-7795, 2012.

867 Ito, A., Sillman, S., and Penner, J. E.: Global chemical transport model study of ozone
868 response to changes in chemical kinetics and biogenic volatile organic compounds
869 emissions due to increasing temperatures: Sensitivities to isoprene nitrate chemistry and
870 grid resolution, *J. Geophys. Res.*, 114, D09301, 2009.

871 Jacob, D. J., and Winner, D. A.: Effect of climate change on air quality, *Atmos. Environ.*,
872 43, 1, 51-63, 2009.

873 Jacobs, M. I., Burke, W. J., and Elrod, M. J.: Kinetics of the reactions of isoprene-derived
874 hydroxynitrates: gas phase epoxide formation and solution phase hydrolysis, *Atmos.*
875 *Chem. Phys.*, 14, 17, 8933-8946, 2014.

876 Jenkin, M. E., Young, J. C., and Rickard, A. R.: The MCM v3.3.1 degradation scheme
877 for isoprene, *Atmos. Chem. Phys.*, 15, 20, 11433-11459, 2015.

878 Kavassalis, S., and Murphy, J. G.: Understanding ozone-meteorology correlations: a role
879 for dry deposition, *Geophys. Res. Lett.* 10.1002/2016GL071791, 2017.

880 Krotkov, N. A., McLinden, C. A., Li, C., Lamsal, L. N., Celarier, E. A., Marchenko, S.
881 V., Swartz, W. H., Bucsela, E. J., Joiner, J., Duncan, B. N., Boersma, K. F., Veefkind, J.
882 P., Levelt, P. F., Fioletov, V. E., Dickerson, R. R., He, H., Lu, Z., and Streets, D. G.:
883 Aura OMI observations of regional SO₂ and NO₂ pollution changes from 2005 to 2015,
884 *Atmos. Chem. Phys.*, 16, 7, 4605-4629, 2016.

885 Lam, Y., Fu, J., Wu, S., and Mickley, L.: Impacts of future climate change and effects of
886 biogenic emissions on surface ozone and particulate matter concentrations in the United
887 States, *Atmos. Chem. Phys.*, 11, 10, 4789-4806, 2011.

888 Lamarque, J.-F., Kyle, G. P., Meinshausen, M., Riahi, K., Smith, S. J., van Vuuren, D. P.,
889 Conley, A. J., and Vitt, F.: Global and regional evolution of short-lived radiatively-active

890 gases and aerosols in the Representative Concentration Pathways, *Clim. Change*, 109, 1,
891 191-212, 2011.

892 Lamsal, L. N., Duncan, B. N., Yoshida, Y., Krotkov, N. A., Pickering, K. E., Streets, D.
893 G., and Lu, Z.: U.S. NO₂ trends (2005–2013): EPA Air Quality System (AQS) data
894 versus improved observations from the Ozone Monitoring Instrument (OMI), *Atmos.*
895 *Environ.*, 110, 130-143, 2015.

896 Lee, B. H., Mohr, C., Lopez-Hilfiker, F. D., Lutz, A., Hallquist, M., Lee, L., Romer, P.,
897 Cohen, R. C., Iyer, S., Kurtén, T., Hu, W., Day, D. A., Campuzano-Jost, P., Jimenez, J.
898 L., Xu, L., Ng, N. L., Guo, H., Weber, R. J., Wild, R. J., Brown, S. S., Koss, A., de
899 Gouw, J., Olson, K., Goldstein, A. H., Seco, R., Kim, S., McAvey, K., Shepson, P. B.,
900 Starn, T., Baumann, K., Edgerton, E. S., Liu, J., Shilling, J. E., Miller, D. O., Brune, W.,
901 Schobesberger, S., D'Ambro, E. L., and Thornton, J. A.: Highly functionalized organic
902 nitrates in the southeast United States: Contribution to secondary organic aerosol and
903 reactive nitrogen budgets, *Proc. Natl. Acad. Sci. U.S.A.*, 113, 6, 1516-1521, 2016.

904 Lee, L., Teng, A. P., Wennberg, P. O., Crounse, J. D., and Cohen, R. C.: On Rates and
905 Mechanisms of OH and O₃ Reactions with Isoprene-Derived Hydroxy Nitrates, *J. Phys.*
906 *Chem. A*, 118, 9, 1622-1637, 2014.

907 Li, J., Mao, J., Min, K.-E., Washenfelder, R. A., Brown, S. S., Kaiser, J., Keutsch, F. N.,
908 Volkamer, R., Wolfe, G. M., Hanisco, T. F., Pollack, I. B., Ryerson, T. B., Graus, M.,
909 Gilman, J. B., Lerner, B. M., Warneke, C., de Gouw, J. A., Middlebrook, A. M., Liao, J.,
910 Welti, A., Henderson, B. H., McNeill, V. F., Hall, S. R., Ullmann, K., Donner, L. J.,
911 Paulot, F., and Horowitz, L. W.: Observational constraints on glyoxal production from
912 isoprene oxidation and its contribution to organic aerosol over the Southeast United
913 States, *J. Geophys. Res.*, 121, 16, 2016JD025331, 2016.

914 Li, Q., Jacob, D. J., Munger, J. W., Yantosca, R. M., and Parrish, D. D.: Export of NO_y
915 from the North American boundary layer: Reconciling aircraft observations and global
916 model budgets, *J. Geophys. Res.*, 109, D2, 2004.

917 Liang, J., Horowitz, L. W., Jacob, D. J., Wang, Y., Fiore, A. M., Logan, J. A., Gardner,
918 G. M., and Munger, J. W.: Seasonal budgets of reactive nitrogen species and ozone over
919 the United States, and export fluxes to the global atmosphere, *J. Geophys. Res.*, 103,
920 D11, 13435-13450, 1998.

921 Lin, M., Horowitz, L. W., Payton, R., Fiore, A. M., and Tonnesen, G.: US surface ozone
922 trends and extremes from 1980 to 2014: quantifying the roles of rising Asian emissions,
923 domestic controls, wildfires, and climate, *Atmos. Chem. Phys.*, 17, 4, 2943-2970, 2017.

924 Liu, X., Zhang, Y., Huey, L. G., Yokelson, R. J., Wang, Y., Jimenez, J. L., Campuzano-
925 Jost, P., Beyersdorf, A. J., Blake, D. R., Choi, Y., St. Clair, J. M., Crounse, J. D., Day, D.
926 A., Diskin, G. S., Fried, A., Hall, S. R., Hanisco, T. F., King, L. E., Meinardi, S.,
927 Mikoviny, T., Palm, B. B., Peischl, J., Perring, A. E., Pollack, I. B., Ryerson, T. B.,
928 Sachse, G., Schwarz, J. P., Simpson, I. J., Tanner, D. J., Thornhill, K. L., Ullmann, K.,
929 Weber, R. J., Wennberg, P. O., Wisthaler, A., Wolfe, G. M., and Ziemba, L. D.:

930 Agricultural fires in the southeastern U.S. during SEAC4RS: Emissions of trace gases
931 and particles and evolution of ozone, reactive nitrogen, and organic aerosol, *J. Geophys.*
932 *Res.*, 121, 12, 7383-7414, 2016.

933 Lockwood, A. L., Shepson, P. B., Fiddler, M. N., and Alaghmand, M.: Isoprene nitrates:
934 preparation, separation, identification, yields, and atmospheric chemistry, *Atmos. Chem.*
935 *Phys.*, 10, 13, 6169-6178, 2010.

936 Lu, Z., Streets, D. G., De Foy, B., Lamsal, L. N., Duncan, B. N., and Xing, J.: Emissions
937 of nitrogen oxides from US urban areas: estimation from Ozone Monitoring Instrument
938 retrievals for 2005-2014, *Atmos. Chem. Phys.*, 15, 10, 14961-15003, 2015.

939 Mao, J., Horowitz, L. W., Naik, V., Fan, S., Liu, J., and Fiore, A. M.: Sensitivity of
940 tropospheric oxidants to biomass burning emissions: implications for radiative forcing,
941 *Geophys. Res. Lett.*, 40, 6, 1241-1246, 2013a.

942 Mao, J., Paulot, F., Jacob, D. J., Cohen, R. C., Crouse, J. D., Wennberg, P. O., Keller, C.
943 A., Hudman, R. C., Barkley, M. P., and Horowitz, L. W.: Ozone and organic nitrates over
944 the eastern United States: Sensitivity to isoprene chemistry, *J. Geophys. Res.*, 118, 19,
945 11,256-211,268, 2013b.

946 Metcalfe, S. E., Whyatt, J. D., Nicholson, J. P. G., Derwent, R. G., and Heywood, E.:
947 Issues in model validation: assessing the performance of a regional-scale acid deposition
948 model using measured and modelled data, *Atmos. Environ.*, 39, 4, 587-598, 2005.

949 Millet, D. B., Jacob, D. J., Boersma, K. F., Fu, T. M., Kurosu, T. P., Chance, K., Heald,
950 C. L., and Guenther, A.: Spatial Distribution of Isoprene Emissions from North America
951 Derived from Dornaldehyde Column Measurements by the OMI Satellite Sensor, *J.*
952 *Geophys. Res.*, 113, D2, 194-204, 2008.

953 Miyazaki, K., Eskes, H., Sudo, K., Boersma, K. F., Bowman, K., and Kanaya, Y.:
954 Decadal changes in global surface NO_x emissions from multi-constituent satellite data
955 assimilation, *Atmos. Chem. Phys.*, 17, 2, 807-837, 2017.

956 Moxim, W., Levy, H., and Kasibhatla, P.: Simulated global tropospheric PAN: Its
957 transport and impact on NO_x, *J. Geophys. Res.*, 101, D7, 12621-12638, 1996.

958 Müller, J. F., Peeters, J., and Stavrakou, T.: Fast photolysis of carbonyl nitrates from
959 isoprene, *Atmos. Chem. Phys.*, 14, 5, 2497-2508, 2014.

960 Nah, T., Sanchez, J., Boyd, C. M., and Ng, N. L.: Photochemical Aging of α -pinene and
961 β -pinene Secondary Organic Aerosol formed from Nitrate Radical Oxidation, *Environ.*
962 *Sci. Technol.*, 50, 1, 222-231, 2016.

963 Naik, V., Horowitz, L. W., Fiore, A. M., Ginoux, P., Mao, J., Aghedo, A. M., and Levy,
964 H.: Impact of preindustrial to present-day changes in short-lived pollutant emissions on
965 atmospheric composition and climate forcing, *J. Geophys. Res.*, 118, 14, 8086-8110,
966 2013.

967 Neuman, J., Parrish, D., Trainer, M., Ryerson, T., Holloway, J., Nowak, J., Swanson, A.,
968 Flocke, F., Roberts, J., and Brown, S.: Reactive nitrogen transport and photochemistry in
969 urban plumes over the North Atlantic Ocean, *J. Geophys. Res.*, 111, D23, 2006.

970 Ng, N. L., Kwan, A. J., Surratt, J. D., Chan, A. W. H., Chhabra, P. S., Sorooshian, A.,
971 Pye, H. O. T., Crounse, J. D., Wennberg, P. O., Flagan, R. C., and Seinfeld, J. H.:
972 Secondary organic aerosol (SOA) formation from reaction of isoprene with nitrate
973 radicals (NO₃), *Atmos. Chem. Phys.*, 8, 14, 4117-4140, 2008.

974 Ng, N. L., Brown, S. S., Archibald, A. T., Atlas, E., Cohen, R. C., Crowley, J. N., Day,
975 D. A., Donahue, N. M., Fry, J. L., Fuchs, H., Griffin, R. J., Guzman, M. I., Herrmann, H.,
976 Hodzic, A., Iinuma, Y., Jimenez, J. L., Kiendler-Scharr, A., Lee, B. H., Luecken, D. J.,
977 Mao, J., McLaren, R., Mutzel, A., Osthoff, H. D., Ouyang, B., Picquet-Varrault, B., Platt,
978 U., Pye, H. O. T., Rudich, Y., Schwantes, R. H., Shiraiwa, M., Stutz, J., Thornton, J. A.,
979 Tilgner, A., Williams, B. J., and Zaveri, R. A.: Nitrate radicals and biogenic volatile
980 organic compounds: oxidation, mechanisms, and organic aerosol, *Atmos. Chem. Phys.*,
981 17, 3, 2103-2162, 2017.

982 Nguyen, T. B., Crounse, J. D., Teng, A. P., St. Clair, J. M., Paulot, F., Wolfe, G. M., and
983 Wennberg, P. O.: Rapid deposition of oxidized biogenic compounds to a temperate
984 forest, *Proc. Natl. Acad. Sci. U.S.A.*, 112, 5, E392-E401, 2015.

985 Nozière, B., Barnes, I., and Becker, K. H.: Product study and mechanisms of the
986 reactions of α - pinene and of pinonaldehyde with OH radicals, *J. Geophys. Res.*, 104,
987 D19, 23645-23656, 1999.

988 Ott, L. E., Pickering, K. E., Stenchikov, G. L., Allen, D. J., DeCaria, A. J., Ridley, B.,
989 Lin, R.-F., Lang, S., and Tao, W.-K.: Production of lightning NO_x and its vertical
990 distribution calculated from three-dimensional cloud-scale chemical transport model
991 simulations, *J. Geophys. Res.*, 115, D4, 2010.

992 Parrish, D., Ryerson, T., Holloway, J., Neuman, J., Roberts, J., Williams, J., Stroud, C.,
993 Frost, G., Trainer, M., and Hübler, G.: Fraction and composition of NO_y transported in
994 air masses lofted from the North American continental boundary layer, *J. Geophys. Res.*,
995 109, D9, 2004.

996 Paulot, F., Crounse, J. D., Kjaergaard, H. G., Kroll, J. H., Seinfeld, J. H., and Wennberg,
997 P. O.: Isoprene photooxidation: new insights into the production of acids and organic
998 nitrates, *Atmos. Chem. Phys.*, 9, 4, 1479-1501, 2009.

999 Paulot, F., Henze, D. K., and Wennberg, P. O.: Impact of the isoprene photochemical
1000 cascade on tropical ozone, *Atmos. Chem. Phys.*, 12, 3, 1307-1325, 2012.

1001 Paulot, F., Jacob, D. J., Pinder, R. W., Bash, J. O., Travis, K., and Henze, D. K.:
1002 Ammonia emissions in the United States, European Union, and China derived by high-
1003 resolution inversion of ammonium wet deposition data: Interpretation with a new

- 1004 agricultural emissions inventory (MASAGE_NH3), *J. Geophys. Res.*, 119, 7, 4343-4364,
1005 2014.
- 1006 Paulot, F., Ginoux, P., Cooke, W. F., Donner, L. J., Fan, S., Lin, M. Y., Mao, J., Naik, V.,
1007 and Horowitz, L. W.: Sensitivity of nitrate aerosols to ammonia emissions and to nitrate
1008 chemistry: implications for present and future nitrate optical depth, *Atmos. Chem. Phys.*,
1009 16, 3, 1459-1477, 2016.
- 1010 Peeters, J., Müller, J.-F., Stavrou, T., and Nguyen, V. S.: Hydroxyl Radical Recycling
1011 in Isoprene Oxidation Driven by Hydrogen Bonding and Hydrogen Tunneling: The
1012 Upgraded LIM1 Mechanism, *J. Phys. Chem. A*, 118, 38, 8625-8643, 2014.
- 1013 Perring, A. E., Bertram, T. H., Wooldridge, P. J., Fried, A., Heikes, B. G., Dibb, J.,
1014 Crounse, J. D., Wennberg, P. O., Blake, N. J., Blake, D. R., Brune, W. H., Singh, H. B.,
1015 and Cohen, R. C.: Airborne observations of total RONO₂: new constraints on the yield
1016 and lifetime of isoprene nitrates, *Atmos. Chem. Phys.*, 9, 4, 1451-1463, 2009.
- 1017 Perring, A. E., Pusede, S. E., and Cohen, R. C.: An Observational Perspective on the
1018 Atmospheric Impacts of Alkyl and Multifunctional Nitrates on Ozone and Secondary
1019 Organic Aerosol, *Chem. Rev.*, 113, 8, 5848-5870, 2013.
- 1020 Philip, S., Martin, R. V., and Keller, C. A.: Sensitivity of chemistry-transport model
1021 simulations to the duration of chemical and transport operators: a case study with GEOS-
1022 Chem v10-01, *Geosci. Model Dev.*, 9, 5, 1683-1695, 2016.
- 1023 Pickering, K. E., Wang, Y., Tao, W. K., Price, C., and Müller, J. F.: Vertical distributions
1024 of lightning NO_x for use in regional and global chemical transport models, *J. Geophys.*
1025 *Res.*, 103, D23, 31203–31216, 1998.
- 1026 Pierce, R. B., Schaack, T., Al-Saadi, J. A., Fairlie, T. D., Kittaka, C., Lingenfelter, G.,
1027 Natarajan, M., Olson, J., Soja, A., Zapotocny, T., Lenzen, A., Stobie, J., Johnson, D.,
1028 Avery, M. A., Sachse, G. W., Thompson, A., Cohen, R., Dibb, J. E., Crawford, J., Rault,
1029 D., Martin, R., Szykman, J., and Fishman, J.: Chemical data assimilation estimates of
1030 continental U.S. ozone and nitrogen budgets during the Intercontinental Chemical
1031 Transport Experiment–North America, *J. Geophys. Res.*, 112, D12, 2007.
- 1032 Pollack, I. B., Ryerson, T. B., Trainer, M., Neuman, J., Roberts, J. M., and Parrish, D. D.:
1033 Trends in ozone, its precursors, and related secondary oxidation products in Los Angeles,
1034 California: A synthesis of measurements from 1960 to 2010, *J. Geophys. Res.*, 118, 11,
1035 5893-5911, 2013.
- 1036 Praske, E., Crounse, J. D., Bates, K. H., Kurtén, T., Kjaergaard, H. G., and Wennberg, P.
1037 O.: Atmospheric Fate of Methyl Vinyl Ketone: Peroxy Radical Reactions with NO and
1038 HO₂, *J. Phys. Chem. A*, 119, 19, 4562-4572, 2015.
- 1039 Pye, H. O. T., Luecken, D. J., Xu, L., Boyd, C. M., Ng, N. L., Baker, K. R., Ayres, B. R.,
1040 Bash, J. O., Baumann, K., Carter, W. P. L., Edgerton, E., Fry, J. L., Hutzell, W. T.,
1041 Schwede, D. B., and Shepson, P. B.: Modeling the Current and Future Roles of

- 1042 Particulate Organic Nitrates in the Southeastern United States, *Environ. Sci. Technol.*, 49,
1043 24, 14195-14203, 2015.
- 1044 Rieder, H. E., Fiore, A. M., Horowitz, L. W., and Naik, V.: Projecting policy - relevant
1045 metrics for high summertime ozone pollution events over the eastern United States due to
1046 climate and emission changes during the 21st century, *J. Geophys. Res.*, 120, 2, 784-800,
1047 2015.
- 1048 Rindelaub, J. D., McAvey, K. M., and Shepson, P. B.: The photochemical production of
1049 organic nitrates from α -pinene and loss via acid-dependent particle phase hydrolysis,
1050 *Atmos. Environ.*, 100, 193-201, 2015.
- 1051 Rindelaub, J. D., Borca, C. H., Hostetler, M. A., Slade, J. H., Lipton, M. A., Slipchenko,
1052 L. V., and Shepson, P. B.: The acid-catalyzed hydrolysis of an α -pinene-derived organic
1053 nitrate: kinetics, products, reaction mechanisms, and atmospheric impact, *Atmos. Chem.*
1054 *Phys.*, 16, 23, 15425-15432, 2016.
- 1055 Rollins, A. W., Kiendler-Scharr, A., Fry, J. L., Brauers, T., Brown, S. S., Dorn, H. P.,
1056 Dubé, W. P., Fuchs, H., Mensah, A., Mentel, T. F., Rohrer, F., Tillmann, R., Wegener,
1057 R., Wooldridge, P. J., and Cohen, R. C.: Isoprene oxidation by nitrate radical: alkyl
1058 nitrate and secondary organic aerosol yields, *Atmos. Chem. Phys.*, 9, 18, 6685-6703,
1059 2009.
- 1060 Rollins, A. W., Smith, J. D., Wilson, K. R., and Cohen, R. C.: Real Time In Situ
1061 Detection of Organic Nitrates in Atmospheric Aerosols, *Environ. Sci. Technol.*, 44, 14,
1062 5540-5545, 2010.
- 1063 Romer, P. S., Duffey, K. C., Wooldridge, P. J., Allen, H. M., Ayres, B. R., Brown, S. S.,
1064 Brune, W. H., Crouse, J. D., de Gouw, J., Draper, D. C., Feiner, P. A., Fry, J. L.,
1065 Goldstein, A. H., Koss, A., Misztal, P. K., Nguyen, T. B., Olson, K., Teng, A. P.,
1066 Wennberg, P. O., Wild, R. J., Zhang, L., and Cohen, R. C.: The lifetime of nitrogen
1067 oxides in an isoprene-dominated forest, *Atmos. Chem. Phys.*, 16, 12, 7623-7637, 2016.
- 1068 Russell, A. R., Valin, L. C., and Cohen, R. C.: Trends in OMI NO₂ observations over the
1069 United States: effects of emission control technology and the economic recession, *Atmos.*
1070 *Chem. Phys.*, 12, 24, 12197-12209, 2012.
- 1071 Sanderson, M., Dentener, F., Fiore, A., Cuvelier, C., Keating, T., Zuber, A., Atherton, C.,
1072 Bergmann, D., Diehl, T., and Doherty, R.: A multi - model study of the hemispheric
1073 transport and deposition of oxidised nitrogen, *Geophys. Res. Lett.*, 35, 17, 2008.
- 1074 Sato, K.: Detection of nitrooxypolyols in secondary organic aerosol formed from the
1075 photooxidation of conjugated dienes under high-NO_x conditions, *Atmos. Environ.*, 42,
1076 28, 6851-6861, 2008.
- 1077 Schwantes, R. H., Teng, A. P., Nguyen, T. B., Coggon, M. M., Crouse, J. D., St. Clair,
1078 J. M., Zhang, X., Schilling, K. A., Seinfeld, J. H., and Wennberg, P. O.: Isoprene NO₃

1079 Oxidation Products from the RO₂ + HO₂ Pathway, *J. Phys. Chem. A*, 119, 40, 10158-
1080 10171, 2015.

1081 Sillman, S.: Ozone production efficiency and loss of NO_x in power plant plumes:
1082 Photochemical model and interpretation of measurements in Tennessee, *J. Geophys. Res.*,
1083 105, D7, 9189-9202, 2000.

1084 Simon, H., Reff, A., Wells, B., Xing, J., and Frank, N.: Ozone Trends Across the United
1085 States over a Period of Decreasing NO_x and VOC Emissions, *Environ. Sci. Technol.*, 49,
1086 1, 186-195, 2015.

1087 Singh, H. B., Brune, W. H., Crawford, J. H., Jacob, D. J., and Russell, P. B.: Overview of
1088 the summer 2004 Intercontinental Chemical Transport Experiment–North America
1089 (INTEX-A), *J. Geophys. Res.*, 111, D24S01, 2006.

1090 Singh, H. B., Salas, L., Herlth, D., Kolyer, R., Czech, E., Avery, M., Crawford, J. H.,
1091 Pierce, R. B., Sachse, G. W., Blake, D. R., Cohen, R. C., Bertram, T. H., Perring, A.,
1092 Wooldridge, P. J., Dibb, J., Huey, G., Hudman, R. C., Turquety, S., Emmons, L. K.,
1093 Flocke, F., Tang, Y., Carmichael, G. R., and Horowitz, L. W.: Reactive nitrogen
1094 distribution and partitioning in the North American troposphere and lowermost
1095 stratosphere, *J. Geophys. Res.*, 112, D12, 2007.

1096 Spittler, M., Barnes, I., Bejan, I., Brockmann, K. J., Benter, T., and Wirtz, K.: Reactions
1097 of NO₃ radicals with limonene and α -pinene: Product and SOA formation, *Atmos.*
1098 *Environ.*, 40, 116-127, 2006.

1099 St. Clair, J. M., Rivera-Rios, J. C., Crounse, J. D., Knap, H. C., Bates, K. H., Teng, A. P.,
1100 Jørgensen, S., Kjaergaard, H. G., Keutsch, F. N., and Wennberg, P. O.: Kinetics and
1101 Products of the Reaction of the First-Generation Isoprene Hydroxy Hydroperoxide
1102 (ISOPOOH) with OH, *J. Phys. Chem. A*, 120, 9, 1441-1451, 2016.

1103 Steiner, A. L., Davis, A. J., Sillman, S., Owen, R. C., Michalak, A. M., and Fiore, A. M.:
1104 Observed suppression of ozone formation at extremely high temperatures due to chemical
1105 and biophysical feedbacks, *Proc. Natl. Acad. Sci. U.S.A.*, 107, 46, 19685-19690, 2010.

1106 Stoeckenius, T. E., Hogrefe, C., Zagunis, J., Sturtz, T. M., Wells, B., and
1107 Sakulyanontvittaya, T.: A comparison between 2010 and 2006 air quality and
1108 meteorological conditions, and emissions and boundary conditions used in simulations of
1109 the AQMEII-2 North American domain, *Atmos. Environ.*, 115, 389-403, 2015.

1110 Stohl, A., Trainer, M., Ryerson, T. B., Holloway, J. S., and Parrish, D. D.: Export of NO_y
1111 from the North American boundary layer during 1996 and 1997 North Atlantic Regional
1112 Experiments, *J. Geophys. Res.*, 107, D11, ACH 11-11-ACH 11-13, 2002.

1113 Strode, S. A., Rodriguez, J. M., Logan, J. A., Cooper, O. R., Witte, J. C., Lamsal, L. N.,
1114 Damon, M., Van Aartsen, B., Steenrod, S. D., and Strahan, S. E.: Trends and variability
1115 in surface ozone over the United States, *J. Geophys. Res.*, 120, 17, 9020-9042, 2015.

1116 Szmigielski, R., Vermeylen, R., Dommen, J., Metzger, A., Maenhaut, W., Baltensperger,
1117 U., and Claeys, M.: The acid effect in the formation of 2-methyltetrols from the
1118 photooxidation of isoprene in the presence of NO_x, *Atmos. Res.*, 98, 2–4, 183-189, 2010.

1119 Tawfik, A. B., and Steiner, A. L.: A proposed physical mechanism for ozone-
1120 meteorology correlations using land–atmosphere coupling regimes, *Atmos. Environ.*, 72,
1121 50-59, 2013.

1122 Teng, A., Crounse, J., Lee, L., St Clair, J., Cohen, R., and Wennberg, P.: Hydroxy nitrate
1123 production in the OH-initiated oxidation of alkenes, *Atmos. Chem. Phys.*, 15, 8, 4297-
1124 4316, 2015.

1125 Tong, D. Q., Lamsal, L., Pan, L., Ding, C., Kim, H., Lee, P., Chai, T., Pickering, K. E.,
1126 and Stajner, I.: Long-term NO_x trends over large cities in the United States during the
1127 great recession: Comparison of satellite retrievals, ground observations, and emission
1128 inventories, *Atmos. Environ.*, 107, 70-84, 2015.

1129 Toon, O. B., Maring, H., Dibb, J., Ferrare, R., Jacob, D. J., Jensen, E. J., Luo, Z. J., Mace,
1130 G. G., Pan, L. L., Pfister, L., Rosenlof, K. H., Redemann, J., Reid, J. S., Singh, H. B.,
1131 Thompson, A. M., Yokelson, R., Minnis, P., Chen, G., Jucks, K. W., and Pszenny, A.:
1132 Planning, implementation and scientific goals of the Studies of Emissions and
1133 Atmospheric Composition, Clouds and Climate Coupling by Regional Surveys
1134 (SEAC4RS) field mission, *J. Geophys. Res.*, 121, 4967-5009, 2016.

1135 Tost, H., Jöckel, P., Kerkweg, A., Pozzer, A., Sander, R., and Lelieveld, J.: Global cloud
1136 and precipitation chemistry and wet deposition: tropospheric model simulations with
1137 ECHAM5/MESSy1, *Atmos. Chem. Phys.*, 7, 10, 2733-2757, 2007.

1138 Trainer, M., Parrish, D. D., Goldan, P. D., Roberts, J., and Fehsenfeld, F. C.: Review of
1139 observation-based analysis of the regional factors influencing ozone concentrations,
1140 *Atmos. Environ.*, 34, 12–14, 2045-2061, 2000.

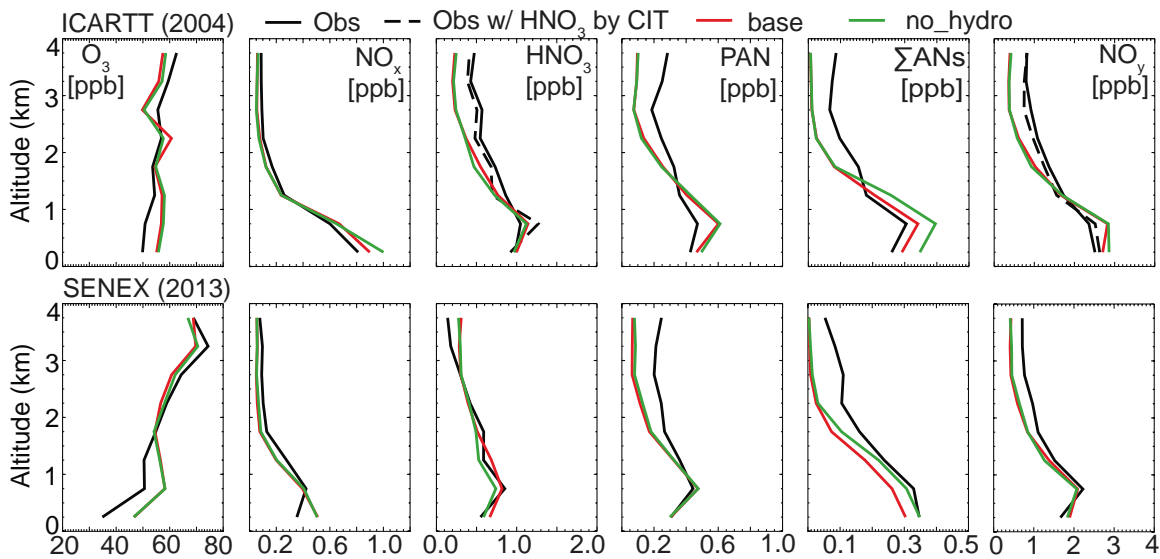
1141 Travis, K. R., Jacob, D. J., Fisher, J. A., Kim, P. S., Marais, E. A., Zhu, L., Yu, K.,
1142 Miller, C. C., Yantosca, R. M., Sulprizio, M. P., Thompson, A. M., Wennberg, P. O.,
1143 Crounse, J. D., St. Clair, J. M., Cohen, R. C., Laughner, J. L., Dibb, J. E., Hall, S. R.,
1144 Ullmann, K., Wolfe, G. M., Pollack, I. B., Peischl, J., Neuman, J. A., and Zhou, X.: Why
1145 do models overestimate surface ozone in the Southeast United States?, *Atmos. Chem.*
1146 *Phys.*, 16, 21, 13561-13577, 2016.

1147 Val Martin, M., Heald, C. L., and Arnold, S. R.: Coupling dry deposition to vegetation
1148 phenology in the Community Earth System Model: Implications for the simulation of
1149 surface O₃, *Geophys. Res. Lett.*, 41, 8, 2988–2996, 2014.

1150 Warneke, C., Trainer, M., de Gouw, J. A., Parrish, D. D., Fahey, D. W., Ravishankara, A.
1151 R., Middlebrook, A. M., Brock, C. A., Roberts, J. M., Brown, S. S., Neuman, J. A.,
1152 Lerner, B. M., Lack, D., Law, D., Hübler, G., Pollack, I., Sjostedt, S., Ryerson, T. B.,
1153 Gilman, J. B., Liao, J., Holloway, J., Peischl, J., Nowak, J. B., Aikin, K. C., Min, K. E.,
1154 Washenfelder, R. A., Graus, M. G., Richardson, M., Markovic, M. Z., Wagner, N. L.,

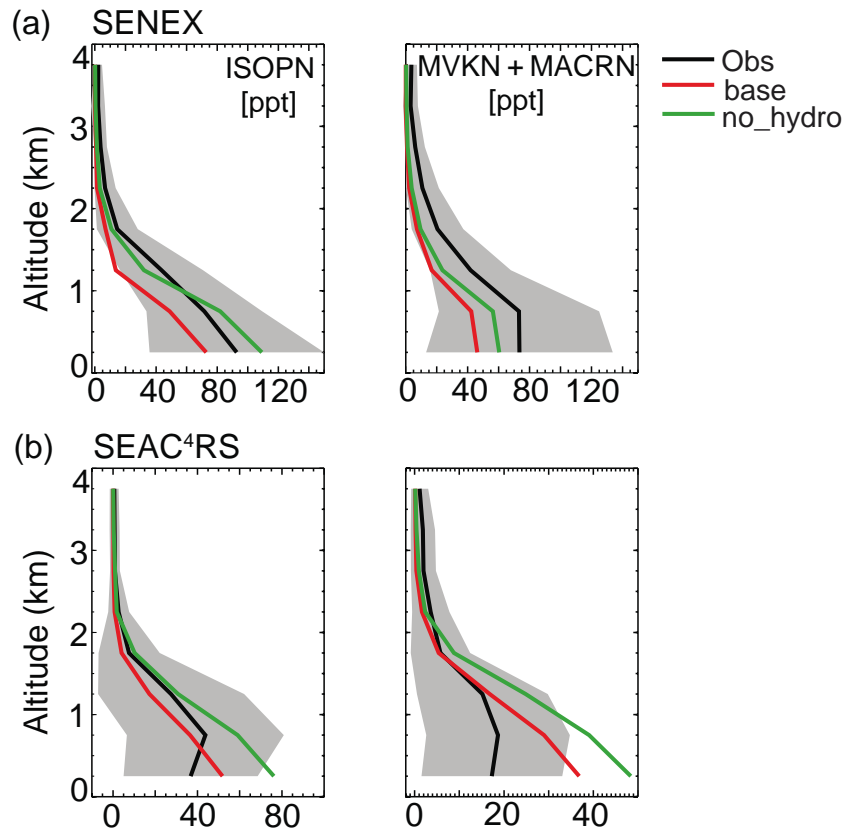
- 1155 Welti, A., Veres, P. R., Edwards, P., Schwarz, J. P., Gordon, T., Dube, W. P., McKeen,
1156 S. A., Brioude, J., Ahmadov, R., Bougiatioti, A., Lin, J. J., Nenes, A., Wolfe, G. M.,
1157 Hanisco, T. F., Lee, B. H., Lopez-Hilfiker, F. D., Thornton, J. A., Keutsch, F. N., Kaiser,
1158 J., Mao, J., and Hatch, C. D.: Instrumentation and measurement strategy for the NOAA
1159 SENEX aircraft campaign as part of the Southeast Atmosphere Study 2013, *Atmos.*
1160 *Meas. Tech.*, 9, 7, 3063-3093, 2016.
- 1161 Wolfe, G., Hanisco, T., Arkinson, H., Bui, T., Crouse, J., Dean - Day, J., Goldstein, A.,
1162 Guenther, A., Hall, S., and Huey, G.: Quantifying sources and sinks of reactive gases in
1163 the lower atmosphere using airborne flux observations, *Geophys. Res. Lett.*, 42, 19,
1164 8231-8240, 2015.
- 1165 Wu, S., Mickley, L. J., Jacob, D. J., Rind, D., and Streets, D. G.: Effects of 2000–2050
1166 changes in climate and emissions on global tropospheric ozone and the policy-relevant
1167 background surface ozone in the United States, *J. Geophys. Res.*, 113, D18312, 2008.
- 1168 Xing, J., Mathur, R., Pleim, J., Hogrefe, C., Gan, C. M., Wong, D. C., Wei, C., Gilliam,
1169 R., and Pouliot, G.: Observations and modeling of air quality trends over 1990–2010
1170 across the Northern Hemisphere: China, the United States and Europe, *Atmos. Chem.*
1171 *Phys.*, 15, 5, 2723-2747, 2015.
- 1172 Xiong, F., McAvey, K. M., Pratt, K. A., Groff, C. J., Hostetler, M. A., Lipton, M. A.,
1173 Starn, T. K., Seeley, J. V., Bertman, S. B., Teng, A. P., Crouse, J. D., Nguyen, T. B.,
1174 Wennberg, P. O., Misztal, P. K., Goldstein, A. H., Guenther, A. B., Koss, A. R., Olson,
1175 K. F., de Gouw, J. A., Baumann, K., Edgerton, E. S., Feiner, P. A., Zhang, L., Miller, D.
1176 O., Brune, W. H., and Shepson, P. B.: Observation of isoprene hydroxynitrates in the
1177 southeastern United States and implications for the fate of NO_x, *Atmos. Chem. Phys.*, 15,
1178 19, 11257-11272, 2015.
- 1179 Xiong, F., Borca, C. H., Slipchenko, L. V., and Shepson, P. B.: Photochemical
1180 degradation of isoprene-derived 4,1-nitrooxy enal, *Atmos. Chem. Phys.*, 16, 9, 5595-
1181 5610, 2016.
- 1182 Xu, L., Suresh, S., Guo, H., Weber, R. J., and Ng, N. L.: Aerosol characterization over
1183 the southeastern United States using high-resolution aerosol mass spectrometry: spatial
1184 and seasonal variation of aerosol composition and sources with a focus on organic
1185 nitrates, *Atmos. Chem. Phys.*, 15, 13, 7307-7336, 2015.
- 1186 Yahya, K., Wang, K., Campbell, P., Glotfelty, T., He, J., and Zhang, Y.: Decadal
1187 evaluation of regional climate, air quality, and their interactions over the continental US
1188 and their interactions using WRF/Chem version 3.6.1, *Geosci. Model Dev.*, 9, 2, 671-
1189 695, 2016.
- 1190 Yienger, J. J., and Levy, H. I.: Empirical model of soil-biogenic NO_x emissions, *J.*
1191 *Geophys. Res.*, 1001, D6, 11447-11464, 1995.
- 1192 Yu, K., Jacob, D. J., Fisher, J. A., Kim, P. S., Marais, E. A., Miller, C. C., Travis, K. R.,
1193 Zhu, L., Yantosca, R. M., Sulprizio, M. P., Cohen, R. C., Dibb, J. E., Fried, A.,

1194 Mikoviny, T., Ryerson, T. B., Wennberg, P. O., and Wisthaler, A.: Sensitivity to grid
1195 resolution in the ability of a chemical transport model to simulate observed oxidant
1196 chemistry under high-isoprene conditions, *Atmos. Chem. Phys.*, 16, 7, 4369-4378, 2016.



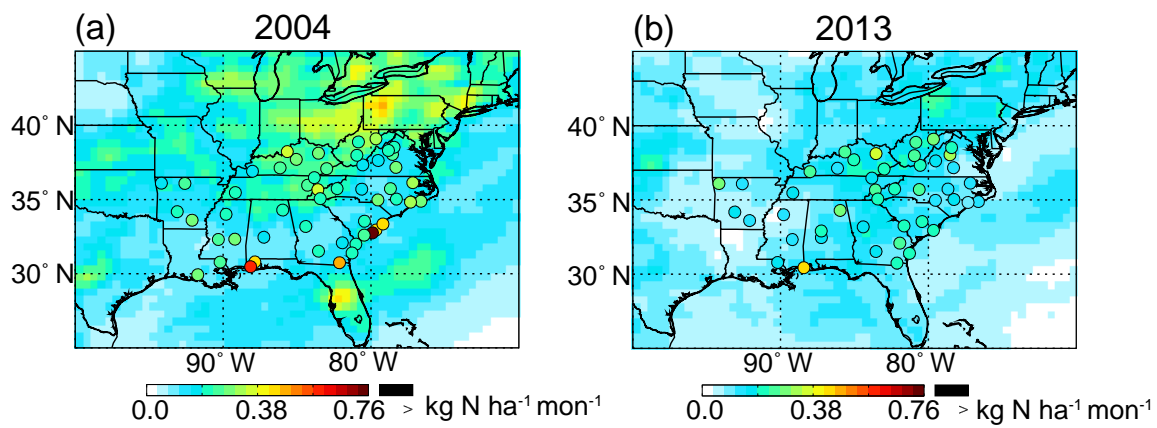
1197

1198 **Figure 1.** Mean vertical profiles of ozone and reactive oxidized nitrogen from observations
 1199 during ICARTT (top row) and SENEX (bottom row) over SEUS (25 - 40° N, 100 - 75° W)
 1200 during daytime, and model estimates from AM3 with hydrolysis of ISOPNB (red) and
 1201 AM3 without hydrolysis of alkyl nitrates (green). The solid and dashed black lines in the
 1202 HNO₃ of ICARTT represent measurements collected using mist chamber/IC by University
 1203 of New Hampshire (UNH) and Chemical Ionization Mass Spectrometer by California
 1204 Institute of Technology (CIT), respectively. NO_y from ICARTT is calculated as the sum of
 1205 NO_x, HNO₃ (w/ UNH in the solid line and w/ CIT in the dashed line), PAN and total alkyl
 1206 nitrates (ΣANs). ΣANs in the bottom row are from SEAC⁴RS.



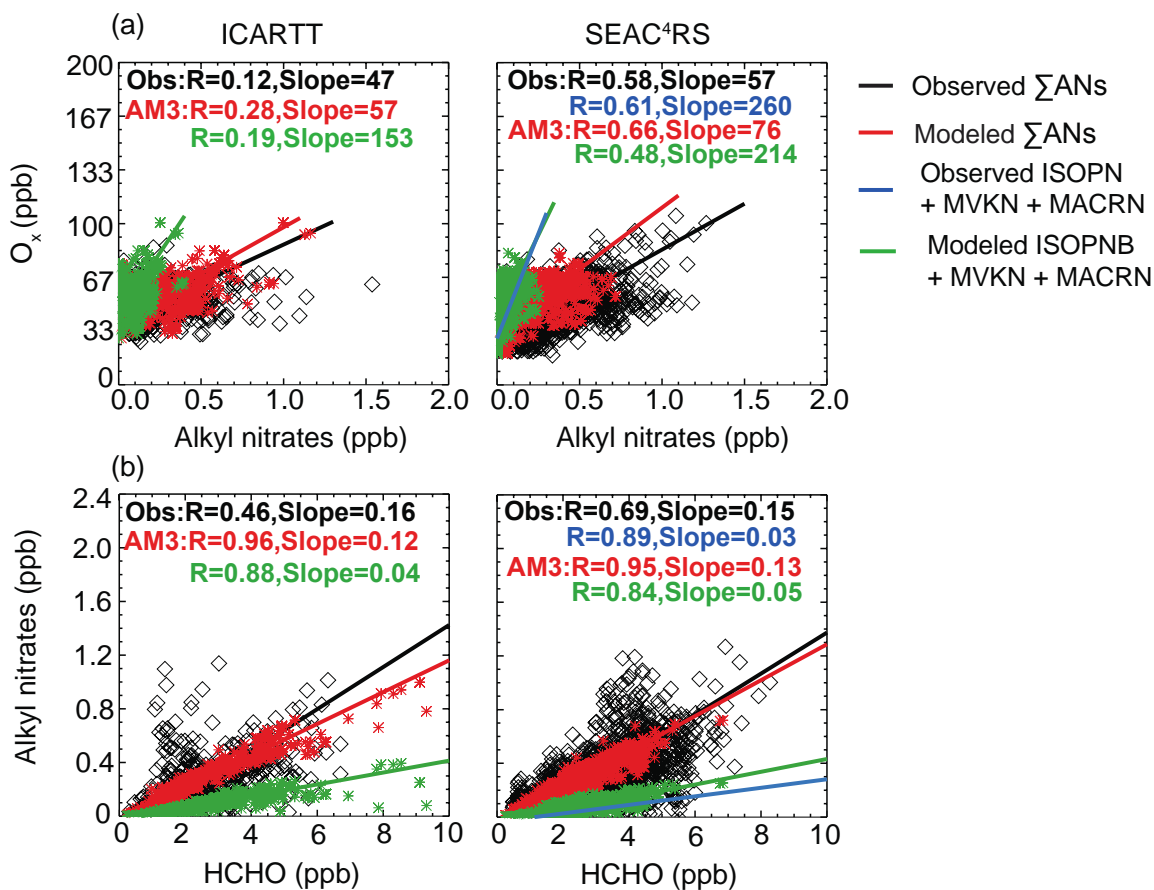
1207

1208 **Figure 2.** Mean vertical profiles of ISOPN and MVKN+MACRN during (a) SENEX and
 1209 (b) SEAC⁴RS over SEUS (25 - 40° N, 100 - 75° W). Black lines are the mean of
 1210 observations. Red and green lines are the mean of modeled results with hydrolysis of
 1211 ISOPNB and without hydrolysis of alkyl nitrates respectively. Grey shades are the one
 1212 standard deviation ($\pm\sigma$) of averaged profiles of the measured tracers.



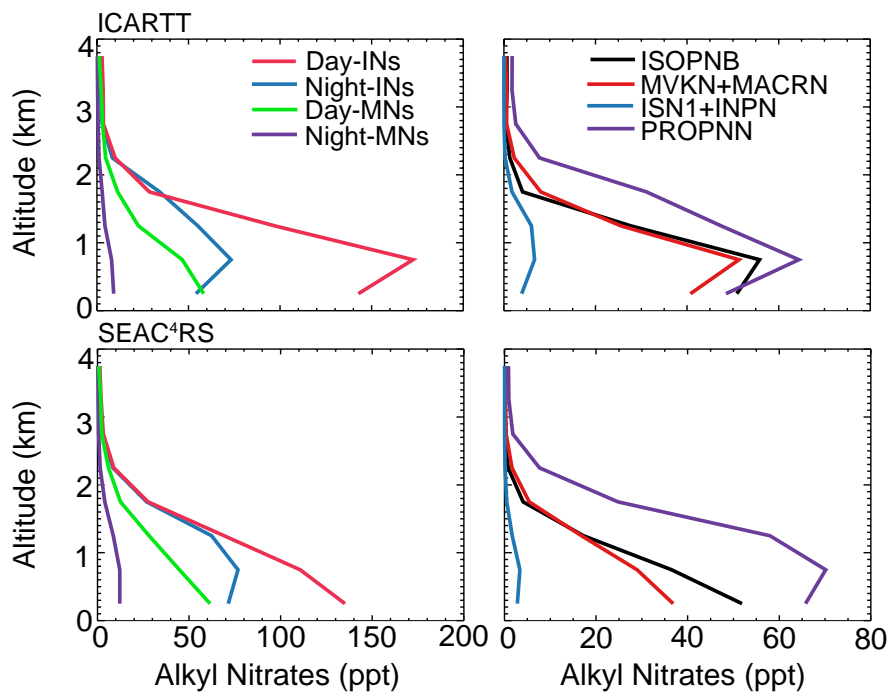
1213

1214 **Figure 3.** Nitrate wet deposition flux ($\text{kg N ha}^{-1} \text{mon}^{-1}$) from NADP (circles) and AM3
 1215 (background) during July - August of 2004 and 2013.



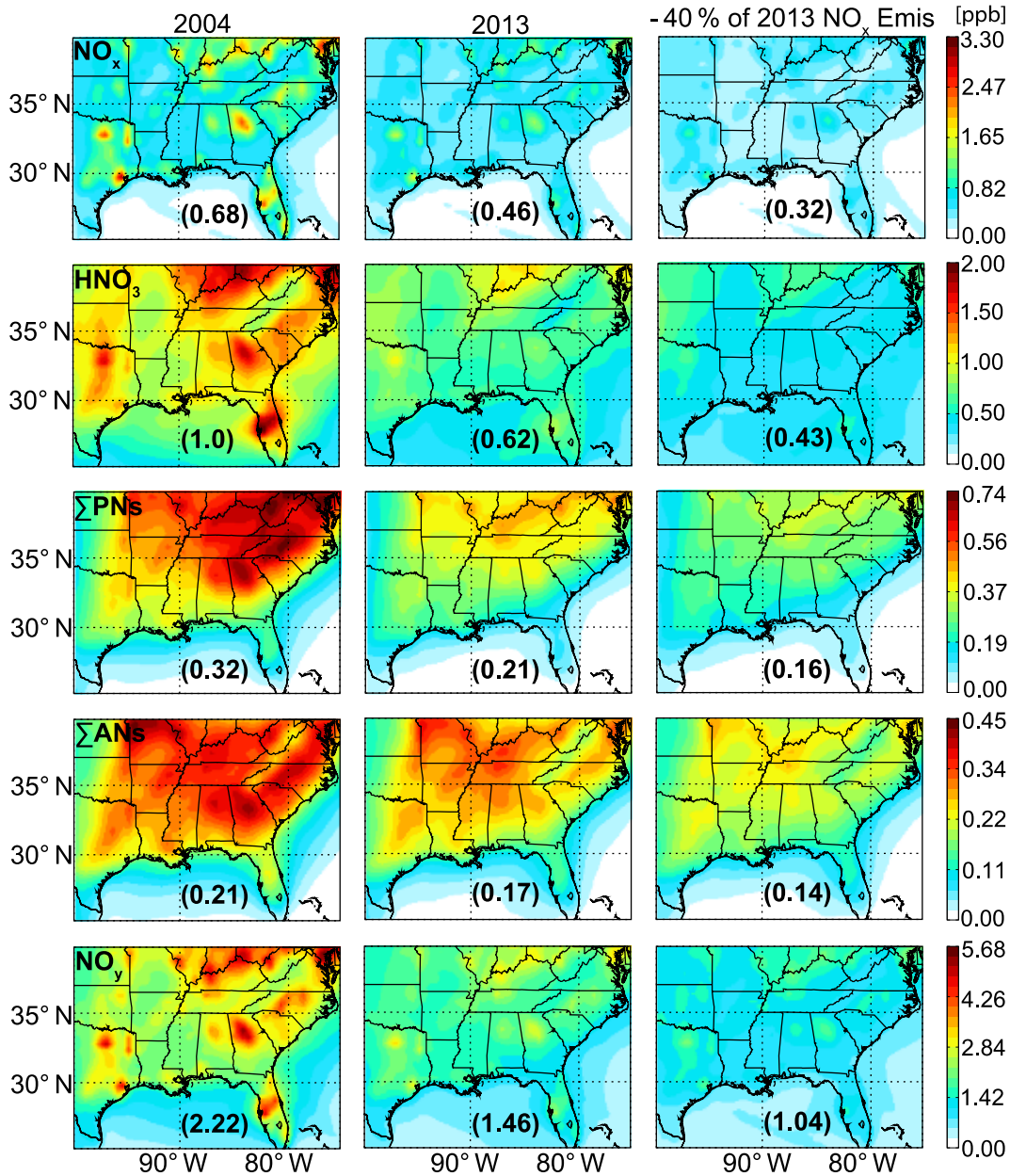
1216

1217 **Figure 4.** O_x versus Σ ANs correlation (top; (a)) and Σ ANs versus formaldehyde
 1218 correlation (bottom; (b)) within the boundary layer (< 1.5 km) during ICARTT (left) and
 1219 SEAC⁴RS (right). Observations are in black diamonds; model estimates from AM3 with
 1220 ISOPNB hydrolysis are in red symbols. Green symbols represent the correlation using
 1221 modeled ISOPN + MVKN + MACRN. Blue symbols represent the correlation using
 1222 observed ISOPN + MVKN + MACRN from SEAC⁴RS. Solid lines are the reduced major
 1223 axis regression lines.



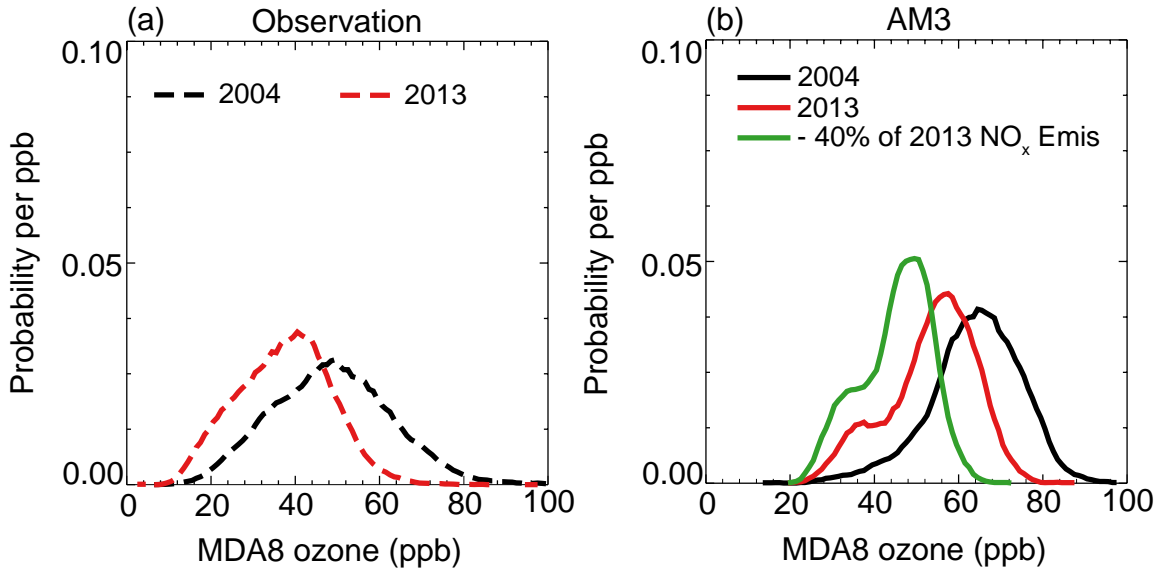
1224

1225 **Figure 5.** Mean vertical profiles of modeled alkyl nitrates from isoprene and monoterpene
 1226 oxidation (left) and major isoprene nitrate species (right) during ICARTT (top row) and
 1227 SEAC⁴RS (bottom row) from AM3 with hydrolysis of ISOPNB.



1228

1229 **Figure 6.** Modeled mean NO_x, HNO₃, total peroxy nitrates (ΣPNs), total alkyl nitrates
 1230 (ΣANs) and NO_y averaged over the boundary layer (< 1.5 km) of the Southeast U.S. during
 1231 July - August of 2004 (left), 2013 (middle), and a scenario assuming 40 % reduction of
 1232 2013 anthropogenic NO_x emissions (right). Numbers in parentheses indicate mean
 1233 concentrations over the plotted region. Note different color scales represent the
 1234 concentration of each species.



1235

1236

1237 **Figure 7.** Observed (a) and simulated (b) probability density function of MDA8 ozone at
 1238 AQS monitoring sites in Figure S3 during summer of 2004, 2013, and a scenario with 40 %
 reduction in the anthropogenic NO_x emissions of 2013.

1239

1240 **Table 1.** Monthly averaged NO_x emissions in July-August of 2004 and 2013 over North
 1241 America (25-50° N, 130-70° W) and over the Southeast US (25-40° N, 100-75° W) in
 1242 brackets in AM3.

Source Type	2004 (Tg N)	2013 (Tg N)
Anthropogenic	0.42 (0.19)	0.25 (0.11)
Biomass Burning	8.4×10^{-3} (2.8×10^{-3})	8.4×10^{-3} (2.8×10^{-3})
Soils	2.9×10^{-2} (9.5×10^{-3})	2.9×10^{-2} (9.5×10^{-3})
Aircraft	8.8×10^{-3} (2.9×10^{-3})	8.0×10^{-3} (2.8×10^{-3})
Lightning	0.02 (0.01)	0.02 (0.01)
Total	0.49 (0.22)	0.32 (0.14)

1243

1244 **Table 2.** Case descriptions

Case name	Heterogeneous Loss of organic nitrates	NO _x emissions	Meteorology
base	ISOPNB with a γ of 0.005 and followed by a hydrolysis rate of $9.26 \times 10^{-5} \text{ s}^{-1}$	2004 and 2013	2004 and 2013
no_hydro	—	2004 and 2013	2004 and 2013
hydro_full	ISOPNB and DHDN with a γ of 0.005 and followed by a hydrolysis rate of $9.26 \times 10^{-5} \text{ s}^{-1}$; TERPN1 with a γ of 0.01 and followed by a hydrolysis rate of $9.26 \times 10^{-5} \text{ s}^{-1}$	2004 and 2013	2004 and 2013
hypo	Same with the base case	40 % reduction of NO _x emissions of 2013	2013

1245

1246 **Table 3.** Monthly NO_y budget in the boundary layer (< 1.5 km) of the Southeast United States for July-August of 2004, 2013 and a
 1247 scenario with 40 % reduction of anthropogenic NO_x emissions of 2013^a.

Species	2004					2013					- 40 % of 2013 Anthropogenic NO _x Emis				
	Emission	Chem (P-L)	Dry Dep	Wet Dep	Net Export	Emission	Chem (P-L)	Dry Dep	Wet Dep	Net Export	Emission	Chem (P-L)	Dry Dep	Wet Dep	Net Export
NO_x	208.7	-172.4	21.8	–	14.5	132.6	-105	14.2	–	13.4	88.3	-69.6	9.2	–	9.5
ΣPNs^b		15.2	5.7	–	9.5		10.3	3.9	–	6.4		7.7	3.0	–	4.7
ΣANs		24.3	14.3	6.2	3.8		19.4	11.4	4.7	3.3		15.4	9.1	3.9	2.4
day ^c		13.8	8.7	3.6	1.5		12.0	7.5	3.0	1.6		10.2	6.3	2.6	1.3
night ^d		10.5	5.6	2.6	2.4		7.4	4.0	1.7	1.7		5.3	2.8	1.3	1.1
HNO₃		131.7	77.8	57.6	-3.7		74.2	45.6	35.1	-6.5		45.8	29.2	25.6	-9.0
NO_y					24.1					16.6					7.6

1248 ^aWe define the boundary of Southeast US is 25-40° N, 100-75° W. All budget terms are in Gg N.

1249 ^bΣPNs includes PAN, peroxyacetyl nitrate (MPAN), and a C5 hydroxy peroxyacyl nitrate (C5PAN1) produced by oxidation of
 1250 ISN1.

1251 ^cAlkyl nitrates produced from oxidation of isoprene and monoterpenes by OH.

1252 ^dAlkyl nitrates produced from oxidation of isoprene and monoterpenes by NO₃.